COMBUSTION TIMING CONTROL OF NATURAL GAS HCCI ENGINES USING PHYSICS-BASED MODELING AND LQR CONTROLLER

A Thesis

by

MARWA WALID FATHY ABDELGAWAD

Submitted to the Office of Graduate Studies of
Texas A&M University
in partial fulfillment of the requirements for the degree of

MASTER OF SCIENCE

May 2012

Major Subject: Mechanical Engineering

Combustion Timing Control of Natural Gas HCCI Engines Using Physics-Based Modeling and LQR Controller

COMBUSTION TIMING CONTROL OF NATURAL GAS HCCI ENGINES USING PHYSICS-BASED MODELING AND LQR CONTROLLER

A Thesis

by

MARWA WALID FATHY ABDELGAWAD

Submitted to the Office of Graduate Studies of
Texas A&M University
in partial fulfillment of the requirements for the degree of

MASTER OF SCIENCE

Approved by:

Co-Chairs of Committee,	Reza Langari
	Reza Tafreshi
Committee Members,	Timothy J. Jacobs
	Deepa Kundur
Head of Department,	Jerald A. Caton

May 2012

Major Subject: Mechanical Engineering

ABSTRACT

Combustion Timing Control of Natural Gas HCCI Engines Using

Physics-Based Modeling and LQR Controller. (May 2012)

Marwa Walid Fathy AbdelGawad, B.Sc., The American University in Cairo

Co-Chairs of Advisory Committee: Dr. Reza Tafreshi
Dr. Reza Langari

Homogeneous Charge Compression Ignition (HCCI) Engines hold promises of being the next generation of internal combustion engines due to their ability to produce high thermal efficiencies and low emission levels. HCCI combustion is achieved through the auto-ignition of a compressed homogenous fuel-air mixture, thus making it a "fusion" between spark-ignition and compression-ignition engines. The main challenge in developing HCCI engines is the absence of a combustion trigger hence making it difficult to control its combustion timing.

The aim of this research project is to model and control a natural gas HCCI engine. Since HCCI depends primarily on temperature and chemical composition of the mixture, Exhaust Gas Recirculation (EGR) is used to control ignition timing. In this research, a thermodynamical, physics-based nonlinear model is developed to capture the main features of the HCCI engine. In addition, the Modified Knock Integral Model (MKIM), used to predict ignition timing, is optimized. To validate the nonlinear model, ignition timing under varying conditions using the MKIM approach is shown to be in accordance with data acquired from a model developed using a sophisticated engine

simulation program, GT-Power. Most control strategies are based on a linear model, therefore, the nonlinear model is linearized using the perturbation method. The linear model is validated by comparing its performance with the nonlinear model about a suitable operating point.

The control of ignition timing can be defined as a regulation process where the goal is to force the nonlinear model to track a desired ignition timing by controlling the EGR ratio. Parameters from the linear model are used to determine the gains of the LQR controller. The performance of the controller is validated by implementing it on the nonlinear model and observing its ability to track the desired timing with 0.5 % error within a certain operating range. To increase the operating range of the controller and reduce steady-state error, an integrator is added to the LQR. Finally, it is shown that the LQR controller is able to successfully reject disturbance, parameter variation, as well as noise.

DEDICATION

To my husband and family

ACKNOWLEDGEMENTS

This thesis is the product of the work and support of several people. I would like to thank my supervisor and co-chair, Dr. Reza Tafreshi, for his support and guidance throughout the course of this research. I am grateful for his patience, diligence and encouragement that he has generously given me. I would also like to thank my co-chair, Dr. Reza Langari for the technical guidance he has given me, as well as the support and care that he and his family offered during my short stay at College Station.

I would like to thank Dr. Timothy Jacobs for teaching me about combustion and for playing a vital role during the course of this research, as well as Dr. Jerald Caton for his technical guidance in thermodynamics.

I would also like to thank Dr. Deepa Kundar for taking the time to read my thesis and provide meaningful feedback.

Furthermore, I would like to thank my colleagues Daniel Zheng, Jiafeng Sun, Yasser Al-Hamidi and Dr. Yujia Zhai for the helpful guidance they provided me during this thesis and for all the helpful discussions. I am especially grateful to Dr. Ebrahimi Behrouz for the technical guidance that he gave me throughout several areas in this research, and for all the time and effort he has offered to help me.

I am also grateful for the financial support of Qatar National Research Fund (QNRF) for funding this project, as well as Texas A&M University at Qatar for the resources that it has provided me to be able to complete my research.

Finally, my most profound thanks go to my husband Ahmad, my mother Faten and my siblings Nada and Mohamed, for pushing me forward, having faith in me and always being there to support me.

NOMENCLATURE

a	Crank radius (m)
A	Arrhenius rate pre-exponential factor (sec^{-1} for a first order reaction, $dm^3\ mol^{-1}\ sec^{-1}$ for a second order reaction)
A_{th}	Arrhenius rate pre-exponential factor $((gmol/cm^3)^{1-a-b}/sec)$
c_p	Specific heat capacities (kJ/K mol)
E_a	Activation energy of the fuel (kJ/mol)
H	Total enthalpy in the cylinder (kJ)
h_{EGR}	Specific enthalpies at intake and exhaust manifolds of EGR (kJ/kg)
$\bar{h}_i(T)$	Molar enthalpy of species i at temperature T (kJ/mol)
$\Delta_f\bar{h}_i$	Molar heat of formation of species i (kJ/mol)
h_{rct}	Specific enthalpies at intake and exhaust manifolds of the reactants (kJ/kg)
k_R	Arrhenius reaction rate
l	Connecting rod length (m)
m	Mass inside cylinder (kg)
$\dot{m}_{EGR}$	Mass flow rate of EGR (kg/s)
$\dot{m}_{rct}$	Mass flow rates of reactants (kg/s)
N_i	Number of moles of species i

$n_{fuel,k}$	Instantaneous number of moles of fuel inside cylinder at engine cycle, k
$n_{O_2,k}$	Instantaneous number of moles of oxygen inside cylinder at engine cycle, k
n_c	Polytropic parameter
P	Pressure (kPa)
Q	Heat transfer (kJ)
r_c	Compression ratio
R_u	Universal Gas Constant (J/K mol)
T	Temperature (K)
U	Internal energy (kJ)
u	Control authority
$V(\theta)$	Volume at angle θ (m^3)
W	Work done (kJ)

Greek Symbols:

α_k	EGR ratio at kth cycle
γ	Ratio of specific heats
ε	Percentage of chemical energy
θ_i	Crank angle at which event i occurs (deg)
ξ	Percentage heat losses due to heat transfer in EGR pipeline
τ	Ignition delay (sec)

φ_k	Equivalence ratio at kth cycle
ω	Engine speed (rad/sec)

Abbreviations:

ARMAX	Autoregressive Moving Average Model with Exogenous Inputs Model
aTDC	After Top Dead Center
CA50	Crank Angle where 50% of total heat release occurs
CAD	Crank Angle Degrees
CFD	Computational Fluid Dynamics
CH_4	Methane
CI	Compression Ignition
CO_2	Carbon Dioxide
CO	Carbon Monoxide
CV	Control Volume
CVA	Canonical Variable Algorithm
DEM	Discrete Event Model
EGR	Exhaust Gas Recirculation
ERL	Exhaust Rebreathing Lift
EVC	Exhaust Valve Closing
EVO	Exhaust Valve Opening
H_2O	Water

HC	Hydrocarbons
HCCI	Homogeneous Charge Compression Ignition
IVC	Intake Valve Closure
KI	Knock Integral
LPV	Linear Parameter Varying
LQG	Linear Quadratic Gaussian
LQR	Linear Quadratic Regulator
MKIM	Modified Knock Integral Model
MIMO	Multi-Input Multi-Output
MISO	Multi-Input Single-Output
MOESP	Multi-variable Output-Error State space model
MPC	Model Predictive Control
MVM	Mean Value Model
N_2	Nitrogen
NO_2	Nitric Dioxide
NO	Nitric Oxide
NO_x	Nitrogen Oxides
O_2	Oxygen
O_3	Ozone
PI	Proportional Integrator
PID	Proportional Integral Derivative
PM	Particulate Matter

RPM	Revolutions Per Minute
RR	Reaction rate
SI	Spark Ignition
SISO	Single-Input Single-Output
SO_2	Sulphur Dioxide
SOC	Start Of Combustion
TDC	Top Dead Center
TKM	Thermo-Kinetic Model
UHC	Unburned HydroCarbons
VAF	Variance-Accounted-For
VVA	Variable Valve Actuation
VVT	Variable Valve Timing

TABLE OF CONTENTS

Page

LIST OF FIGURES

FIGURE Page

FIGURE Page

LIST OF TABLES

1. INTRODUCTION

1.1 Motivation

For many years researchers have been trying to develop internal combustion engines with increased efficiency, while striving to satisfy stricter environmental regulations. Emissions caused by internal combustion engines have affected the environment significantly and impacted the health of the human population. These emissions are combustion by-products made up of hydrocarbons (HC), nitrogen oxides (NO_x), sulphur dioxide (SO_2), carbon monoxide (CO), carbon dioxide (CO_2) and particulate matter (PM). Toxic gases such as CO, NO_x, and HC are the causes of health hazards caused by emissions.

CO is known to readily react with hemoglobin in the blood more than oxygen and hence impeding the transportation of oxygen around the body [1]. NO_x are associated mainly with nitric oxide (NO) and nitrogen dioxide (NO_2). Reactions between NO_x and volatile HCs lead to the formation of ozone (O_3). While ozone in the atmosphere is beneficiary because it absorbs the Sun's harmful ultra-violet rays, ground-level ozone, also known as "smog", is actually harmful. Ozone has proven to cause respiratory illnesses, decrease lung functionality by more than 15%, with an increased effect on asthmatic patients [1]. HCs such as benzene, formaldehyde, and acetaldehyde are also responsible in affecting the human health, and have been classified as carcinogenic [1].

This thesis follows the style of Journal of Dynamic Systems, Measurement, and Control.

The environmental impact of combustion emissions is caused by the presence of PM or "soot" and SO_2. Particulate matter can reduce visibility by absorbing or scattering light. This is the cause of the "black cloud" that is seen covering highly-polluted areas. Moreover, PM has proven to cause respiratory illnesses, cardiovascular diseases and sometimes even death [1]. SO_2, in addition to NO_x, are both responsible for the formation of acid rain when reacted with water and oxygen in the atmosphere. Acid rain has a damaging effect on buildings, agriculture, and marine life.

Due to the hazardous effects of emissions on the environment and human health, the Environmental Protection Agency has found it necessary to restrict regulations on the emission levels of passenger vehicles [2,3]. Posing as a challenge to the vehicle industry, alternative options needed to be explored which included more efficient and cleaner engines. Homogeneous Charge Compression Ignition (HCCI) engines have provided a window of opportunity to make this happen.

1.2 Background

1.2.1 HCCI Fundamentals

HCCI Combustion was first studied by Onishi et al. [4] in 1979. An HCCI engine has incorporated features from both the conventional spark ignition (SI) gasoline engine and the compression ignition (CI) technology of the diesel engine. A gasoline SI engine depends on igniting a homogeneous fuel-air mixture using a spark plug during the end of the compression cycle. On the other hand, in a diesel engine, air is compressed in the cylinder during the compression cycle and combustion is triggered when a combustible fuel is injected into the cylinder. Due to the high temperature and high pressure of the air

during its compression, the air and injected fuel are mixed and ignited. In HCCI engines, a charge of homogeneous fuel-air mixture goes into the cylinder, as in SI engines, but the mixture is ignited by compression as in CI engines. The major attribute of a HCCI engine, in comparison with a SI or CI engine, is that it does not have a direct trigger to start the combustion process. SI engines start combustion with the use of a spark plug while CI engine combustion commences when the fuel is injected into the chamber. A HCCI engine's combustion depends solely on the chemical-kinetic reaction of the fuel-air mixture inside the chamber [5]. Figure 1.1 shows the difference in combustion methods between SI, CI and HCCI engines [6].

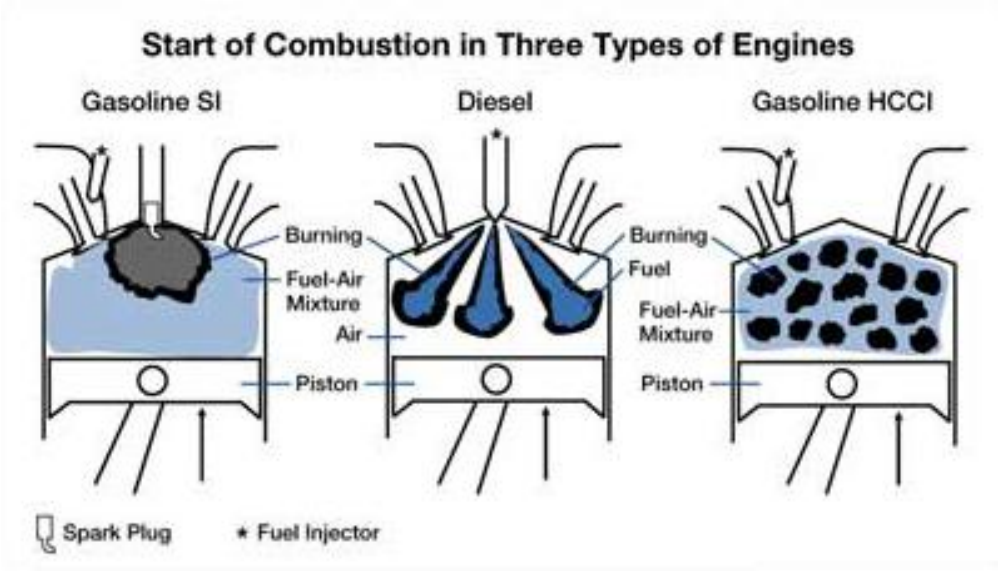

Figure 1.1 Combustion modes of three types of engines (Gasoline SI, Diesel CI, and HCCI)

HCCI engines hold the advantages of both SI and CI engines. In SI engines, the advantage of having a homogeneous fuel-air mixture results in a uniform compression

and relatively “clean” combustion with low emissions of NO_x. However, SI engines cannot operate on high compression ratios because they are at risk of “knocking”. Knocking occurs due to the further compression of the unburned residual mixture causing it to auto-ignite, hence causing a "knocking effect". A rapid increase in pressure in SI engines may damage the spark plugs and oil gaskets [7]. On the other hand, a CI engine has high efficiency due to the high compression ratio since CI engines are compressing only air, instead of a fuel-air mixture. CI engines are also known to have high efficiency and low reaction temperatures because they can operate on lean mixtures [7]. However, CI engines produce more particulate and NO_x emissions since the fuel-air mixture is not pre-mixed and homogeneous as in SI engines [8].

By combining the advantages of using a homogeneous mixture of fuel and air as in a SI engine, and igniting the mixture using compression as in CI engines, HCCI engines result in higher efficiencies in comparison with a conventional SI engine, due to the high compression ratio and the lean mixture of air and fuel. Moreover, HCCI engines produce cleaner emissions since they intake a homogeneous mixture of fuel and air, as in SI engines, which can be very lean and therefore decreasing the amount of NO_x and particulate matter in emissions. Unfortunately, CO and unburned hydrocarbons (UHC) are emissions that are still resultants of a HCCI combustion process since combustion is occurring at low temperatures. Table 1.1 compares the characteristics of SI and CI engines, while highlighting the attributes that were "inherited" when converting to HCCI combustion.

Table 1.1 Comparison of certain engine parameters for SI, CI and HCCI engines

	SI	CI	HCCI
Compression Ratio (Approx. range)	7 – 11.5	12 – 20	15 – 24
Fuel(s) Used	Gasoline, Ethanol, Hydrogen, Natural Gas, Liquid Petrol Gas	Diesel, Biodiesel, Liquid Petrol Gas, Natural Gas	Gasoline, Diesel, Biodiesel, Liquid Petrol Gas, Natural Gas
Degree of Mixing	Homogeneous	Heterogeneous	Homogeneous
Equivalence Ratio	$\varphi = 1$	$0.15 \leq \varphi \leq 0.8$	$0.15 \leq \varphi \leq 0.5$
Method of Ignition	Spark Ignition	Compression Ignition	Compression Ignition

1.2.2 Challenges Associated with HCCI Implementation

Although HCCI engines might seem like the ultimate solution to solve the issue of non-environmentally friendly emissions, they are not a solution without drawbacks. The main challenge impeding the introduction of HCCI engines into the global market is the control of combustion timing. Since HCCI engines depend primarily on auto-ignition, there is no direct trigger to start the combustion process except the thermochemical path of the mixture. Therefore, ignition depends on the temperature and pressure of gas mixtures from previous cycles. To be able to operate a HCCI engine efficiently, the combustion timing must be controlled. Early combustion could lead to undesirable pressure levels within the cylinder which may result in knocking, causing loud noise and eventually damaging the engine . On the other hand, late combustion

could lead to misfires or incomplete combustion and therefore resulting in an increase in CO emissions and unburned hydrocarbons.

HCCI implementation is the other major challenge. Two of the most common techniques to achieve HCCI are (1) re-inducting exhaust gases back into the cylinder, known as Exhaust Gas recirculation (EGR), and (2) trapping them inside the cylinder. By mixing the residual gases with the freshly inducted fuel/air mixture, the temperature and chemical composition of the next engine cycle are altered. This is called cycle-to-cycle coupling and needs to be taken into consideration since it affects steady state and mode transitions. Other ways to implement HCCI combustion and control combustion timing will be further discussed in the following subsection.

1.3 Previous Related Work

Several attempts have been made to control ignition timing in HCCI engines. In order to implement a certain control technique, a model needs to be developed before designing the controller. This section provides an overview of the different models that were researched, as well as the different control techniques that were implemented.

1.3.1 HCCI Modeling Techniques

Two main techniques are used when modeling HCCI engines: thermo-kinetic models and control-oriented models. Thermo-kinetic models depend on thermodynamical and chemical relationships. Control-oriented models depend on ignition timing correlations, as well as physics-based and system identification techniques.

1.3.1.1 HCCI Thermo-Kinetic Models

HCCI combustion largely relies on chemical kinetics therefore they must be integrated within the mathematical model. Modeling approaches can be categorized as follows depending on the complexity and the details of the kinetics included (from the least to the most complex) [8]:

1. Zero-dimensional Thermo-Kinetic Models (TKM)
2. Multi-zone thermo-kinetic models
3. Sequential Computational Fluid Dynamics (CFD) based multi-zone thermo-kinetic models
4. Fully Coupled CFD thermo-kinetic models

Zero-dimensional (single-zone) thermo-kinetic models assume that the control volume being studied is made up of one zone in which the in-cylinder temperature and fuel-air mixture concentration is homogeneous. By assuming homogeneity, the modeling process is simplified resulting in low order kinetic mechanisms with low computational requirements. Usually the first law of thermodynamics is applied to the control volume to determine pressure and/or temperature, in addition to valve flow equations that are used to determine gas composition, which is a similar approach used by Shaver et al. [9]. Examples where other types of single-zone TKMs were used are found in [10-12]. Due to inaccurate estimates of residual temperatures and composition, single-zone TKM models are unable to provide accurate predictions of rate of heat release, emissions, as well as track transient responses.

In an attempt to resolve some of the shortcomings of zero-dimensional models in predicting emissions and engine performance, while avoiding an increase in computational demands, multi-zone thermo-kinetic models were developed. Such models divide the control volume to several zones, considering each as a zero-dimensional TKM, rather than treating it as one single zone. Each zone has its own independently defined initial conditions of the various parameters. Mass exchange and heat transfer relationships can be taken into consideration. Models depending on multi-zone TKMS vary in the way the zones are defined either by their number, kind (e.g. adiabatic core zones, boundary layers, crevices) and type of zone-interactions (e.g. pressure-volume work, heat transfer, mass exchange) [8]. For example, Fiveland and Assanis [13,14] developed a model that included an adiabatic core, a thermal boundary layer model and a crevice region. Since boundary layers and crevices are taken into consideration, multi-zone TKMs can give a better prediction of emission levels compared to zero-dimensional TKMs although it is more complex. Aceves et al. [5] and Kongsereeparp et al. [15] both developed a single-zone and a multi-zone model in order to highlight the advantages of using each model.

Zero-dimensional and multi-zone TKMS both evaluate in-cylinder processes occurring only while the valves are closed, i.e. from intake valve closure (IVC) to exhaust valve opening (EVO), as opposed to CFD based multi-zone TKM. Sequential CFD based multi-zone models aim to include the same processes in addition to the modeling of air and fuel intake and exhaust gases being released from the engine [16,17]. Processes that are occurring between IVC and EVO can then be modeled using

either single-zone or multi-zone TKMs. Overall, this approach is more complex since the "homogeneous" assumption used in single-zone or multi-zone TKMs is no longer valid. However, this model can demonstrate that low-temperature regions along the cylinder wall and ring crevice cause combustion inefficiency, unburned hydrocarbons and CO emissions.

Finally, multi-dimensional CFD-TKMs are considered to be the most complex of all four models requiring the most computational time. In such models, fluid mechanics and chemical kinetics are coupled together in 3D space where they run in parallel to evaluate any engine process. This allows the user to fully capture the effects of the combustion process on the fluid and vice versa. Agarwal and Assanis [18,19] used detailed chemical kinetic mechanisms in parallel with KIVA-3V which is a multi-dimensional fluid mechanics code to explore the auto-ignition of natural gas.

1.3.1.2 HCCI Control-Oriented Models

For control design purposes, low-order models with short computation time are usually desired. Therefore, several control-oriented models were developed in an attempt to control combustion timing. Control models are usually divided into two main categories: steady-state models and cycle-to-cycle (transient) models.

Steady-state models are useful when attempting to model the combustion timing during steady-state conditions. Two main steady state models are Mean Value Model (MVM) and Discrete Event Model (DEM). Mean value models are continuous in time and study mean-value descriptions of changes that occur during combustion, such as cycle-average cylinder flows, instead of a detailed description of the in-cylinder

processes. Since the events occurring within the engine cycle are not being studied, then the independent variable here is time and not crank angle [20]. In [21] a MVM was used to control the air-fuel ratio and combustion timing of an HCCI engine by regulating EGR and Exhaust Rebreathing Lift (ERL). The crank angle at which 50% of fuel is burnt (CA50) is used to evaluate when combustion occurs. Since this is a mean-value model, the cylinder was modeled as a pump based on average values of cylinder flows throughout the cycle and exhaust temperature samples taken at each cycle.

On the other hand, DEMs are discrete and take into account events occurring within a full engine cycle by dividing the cycle into stages and analyzing each stage. Therefore the independent variable becomes the crankshaft angle instead of time [20]. There are several types of DEMs such as Variable Valve Actuation (VVA), temperature threshold, Knock Integral Models (KIM) and Arrhenius-type expressions [20]. Some of these models were incorporated together to result in modified models such as Modified Knock Integral Models (MKIM) [22] and Integrated Arrhenius Rate Threshold which involves the knock integral condition $\int_{t=0}^{t_i} \frac{dt}{\tau} = 1$, where t_i is the initial time of ignition and τ is the estimated ignition delay at instantaneous temperature and pressure at time t. Ignition delay is found using Arrhenius-type expressions [11].

Other steady-state models include double-Wiebe function combustion model, empirical look-up table approach and Shell model [22]. The look-up table approach requires considerable effort in order to calibrate it with the experimental setup while it does not take into account physical engine properties [11]. However, Shell model is an

alternative that is widely used. Using a lumped chemical kinetics model, the Shell model predicts auto-ignition without having to model the whole combustion process [11].

Steady-state models usually provide an average value for the combustion timing without taking into consideration dynamics of cycle-to-cycle transitions. However, they can be merged with other models to consider cyclic interactions [23,24]. These are known as cycle-to-cycle models and are used to handle the transitional stages that are experienced throughout the combustion process. For example, transition between different load-speed regions and mode transition between HCCI operation and SI and CI operations [22]. There are two main approaches for transient models: physics-based modeling and system identification-based modeling [22].

Physics-based models are models that depend on the thermodynamics of the combustion process and include exhaust/residual thermal feedback between each cycle. Examples of physics-based models were developed in Shaver et al. [9,24,25] and Chiang et al. [26] where both had engine running conditions as the inputs, e.g. revolutions per minute (RPM), initial temperature, and initial pressure. Using an experimental setup, Shaver et al. [9,24] compares three steady-state combustion models: temperature threshold, integrated Arrhenius expression and KIM. The Arrhenius expression proved the closest to match the experimental data. The selected combustion model was then integrated into a physics-based model, that was developed based on a first-law thermodynamic analysis of the cylinder and exhaust manifold, to predict HCCI combustion timing. Shaver's model considered peak pressure, fuel/air equivalence ratio at peak pressure and work output as the model outputs, while Chiang's model had Start

of Combustion (SOC) and CA50 as the model's outputs [22]. Shahbakhti et al. [23] extended the mean-value model to a full-cycle simulation to develop a physics-based model.

On the other hand, system identification-based modeling is based on considering the system as a black box and using statistical methods to build mathematical models from measured data. In addition, validation models are required to verify the estimation models achieved through system identification methods. Examples of the most well-known system identification models are Autoregressive Moving Average Model with Exogenous Inputs Model (ARMAX) [27], Least-squares [28], Maximum Likelihood [29], and Subspace-based models such as Multi-variable Output-error State Space Model (MOESP) and Canonical Variable Algorithm (CVA) [30, 31]. Examples of models used for validation are residual analysis, cross-validation, one-step-ahead prediction and Variance-Accounted-For (VAF). In [30] and [31], all these methods were applied for validation.

Most processes in HCCI engines are Multi-Input Multi-Output (MIMO) processes. However, during the identification of models, it is often easier to simplify the process. Two main approaches have been used: converting the MIMO process into a Multi-Input Single-Output (MISO) process by just taking into consideration one output as a reliable indication of combustion [31], or linearizing the obtained nonlinear model [30]. Although linearizing the system simplifies the problem and helps in identifying the model, linearized models are only valid about the operating points at which they are linearized.

1.3.2 HCCI Control Techniques

Most HCCI control methods use closed-loop control to adjust ignition timing. As previously mentioned, HCCI engines do not have direct control over ignition timing; therefore, several methods have been proposed as a way to "indirectly" control ignition by controlling other parameters such as:

- Intake temperature [5,20,32,33]
- Compression ratio [34,35]
- Variable Valve Timing (VVT) [36,37,38]
- Intake pressure [39,40]
- Variable EGR [41,42,43]
- Fuel mixture alterations (dual fuel, fuel composition, equivalence ratio) [44, 45]

After choosing the method of control, a controller scheme must be chosen. Several controller schemes used by researchers include Proportional Integral Derivative (PID), Linear Quadratic Gaussian (LQG), Model Predictive Control (MPC), and Linear Quadratic Regulator (LQR). Haraldsson et al. [35] used a PID controller to control the average combustion timing of a five-cylinder engine. In addition, each cylinder had its own PID controller to control the air-fuel ratio. Strandh et al. [31] developed a LQG controller using a model that was derived by MOESP system identification. The performance of the LQG controller was compared to that of a PID controller and both succeeded in controlling the HCCI engine. Furthermore, the model used a feedforward filter and the performance of both controllers was compared both with and without the filter. Adding the feedforward filter increased the operating range of both controllers but

reduced their step response performance. Killingsworth [33] also used a feedforward controller with an added integrator to control HCCI combustion timing. However, to model combustion timing, a different approach was used which depended on an ignition line that is a function of motored temperature and pressure. Killingsworth found that, for natural gas, HCCI ignition timing falls on a line as in-cylinder temperature and pressure were varied. Therefore, ignition timing can be modeled as a linear relationship between in-cylinder temperature and pressure. Olson et al. [46] used fuel mixture alteration as the control technique where two fuels with different octane numbers were mixed to vary the overall octane number. Gain-scheduled PID controllers were used to regulate the octane number of the fuel entering each cylinder and therefore controlling the combustion timing of the engine.

Bengtsson et al. [30] used MPC to control a heavy duty HCCI engine with variable valve actuation. The goal was to minimize fuel consumption and emissions while maintaining a certain in-cylinder pressure. Agrell et al. [38] used a Proportional Integral (PI) controller to actuate the valve timings of a single-cylinder engine to control combustion timing. A feedfoward controller consisting of an ignition model based on the knock integral was later added in [47]. Shaver et al. [48] linearized the ten-state physics-based nonlinear model they developed in [24] to be able to develop a LQR control law. A decoupled control scheme with different time scales [49] was then developed based on dynamic feedback linearization [50] to control in-cylinder peak pressure as well as combustion timing. Ravi et al. [51] used a similar approach [48,50], however, an observer was added to the LQR controller. The observer was used to estimate the states:

moles of oxygen in exhausted products and temperature of trapped exhaust at Exhaust Valve Closing (EVC), since they could not be directly measured from the experimental setup.

In conclusion, several techniques have been developed to model and control HCCI engines. If the aim is to model combustion kinetics chemically and thermodynamically, then one of the TKMs explained above can be used depending on the degree of accuracy required and the parameters under consideration. On the other hand, if the goal is to control HCCI engines, then a control-oriented model will be implemented. The method of HCCI control will depend on the experimental apparatus and how HCCI is achieved, e.g. by increasing intake temperature, altering the compression ratio, re-inducting exhaust gases, etc. The next step would be to select the controller scheme which will depend on the type of model that has been previously developed.

1.4 Objective

Natural gas is seen as a promising alternative fuel for engines since it produces less harmful emissions when burnt and still provides high efficiencies. Qatar has the world's third largest natural gas reserve with a majority of its total energy consumption coming from natural gas, approximately 75% in 2008 [52].

As such, the objective of this thesis is to model and control the combustion timing of an HCCI natural gas engine to ensure maximum efficiency while maintaining low-emission levels. EGR and altering the intake temperature are the primary techniques that will be used to control start of combustion. To model the dynamics of the HCCI

engine, the MKIM correlation for ignition timing will be incorporated into a physics-based nonlinear model. Furthermore, LQR controller will be used to control the EGR ratio and intake temperature.

1.5 Thesis Outline

The outline of the contents of the thesis is as follows:

In *Section 2*, a physics-based nonlinear model of a natural gas fueled HCCI engine is developed. This model uses the MKIM correlation to model the start of combustion and thermodynamical relationships to model the rest of the processes occurring within the engine cycle. The use of EGR ratio and intake temperature to control combustion timing is demonstrated.

In *Section 3*, a nonlinear input-output relationship is developed based on the nonlinear model obtained in Section 2. The relationship is linearized using the perturbation method since a linear control scheme, LQR, will be used to develop the controller for ignition timing.

Section 4 gives an insight on the theory behind LQR controllers and why they are suitable for this project. The development of the LQR controller is demonstrated and its robustness tested when implemented on the linear model. The LQR controller is then applied to the nonlinear model and its performance validated. In addition, the ability of the LQR controller to reject different types of disturbances was studied.

In *Section 5* the work presented in this thesis is summarized and areas for future study are discussed.

2. DEVELOPMENT OF A PHYSICS-BASED CONTROL MODEL

There are various types of modeling techniques that could be used to model the processes occurring throughout the engine cycle. As discussed in Section 1.3.1, only a few models could be used for control purposes, those with less complexity and shorter computation time. Therefore, to control combustion timing, steady-state models are used in parallel with transient models to consider cycle-to-cycle transitions. In this section, the steady state model used for combustion timing, the Modified Knock Integral Model (MKIM), is incorporated within a physics-based model that is developed based on the thermodynamics of the engine cycle.

2.1 Thermodynamic Modeling Approach

An HCCI engine is assumed to have a thermodynamic cycle that is similar to the Otto cycle where combustion is considered to occur at constant volume. Although, this assumption is very rigid, it is valid in HCCI engines because combustion occurs through auto-ignition of a compressed mixture. Hence, burning of the mixture can be assumed to occur “instantaneously”, i.e. at constant volume.

The engine cycle starts with a surge of fresh intake air and fuel, which in this case is natural gas, mixed homogeneously together with external Exhaust Gas Recirculation (EGR) inside the intake adapter. The final mixture is preheated before it enters the cylinder. As the induction stroke begins, the intake valve opens and the cylinder piston moves downward towards the bottom dead center to draw the heated mixture into the cylinder chamber. The intake valve closes and the cylinder moves

upward compressing the mixture. The compression stroke triggers the auto-ignition of the mixture which usually occurs close to the top dead center. Once the mixture starts to combust, chemical energy is transformed into mechanical energy pushing the cylinder downwards and expanding the volume inside the cylinder leading to the expansion stroke. The exhaust valve opens when the cylinder reaches close to the bottom dead center and the cylinder pushes the exhaust gases resulting from the combustion outside the cylinder chamber, hence commencing the exhaust stroke. The intake valve opens followed by the closure of the exhaust valve starting the induction phase once again. The four strokes of the engine cycle are shown in Figure 2.1 below [33].

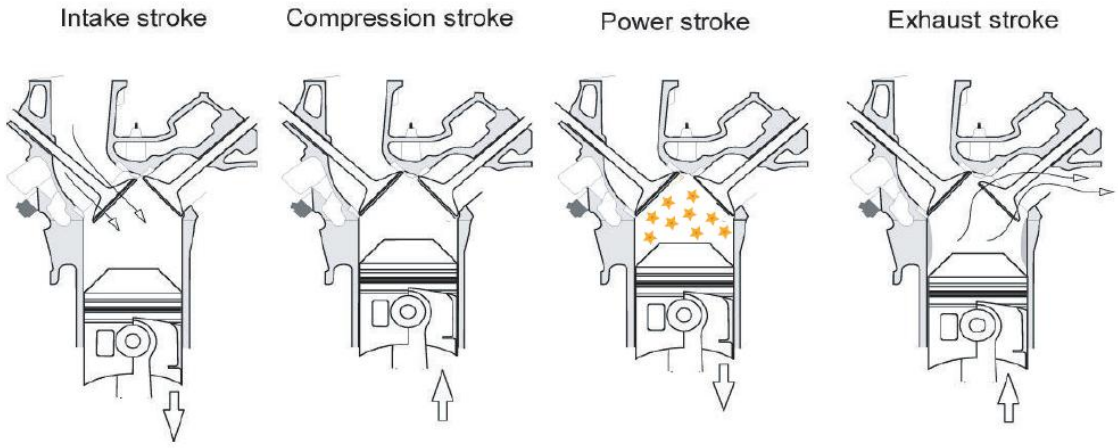

Figure 2.1 The four strokes in an HCCI engine cycle

The engine cycle can also be seen as an ideal thermodynamical cycle divided into five processes:

1- Constant pressure, adiabatic induction of a *lean* mixture of fresh reactants and external EGR

2- Isentropic compression until pre-combustion stage or start of combustion (SOC)

3- Constant volume combustion

4- Isentropic expansion until exhaust valve opens (EVO)

5- Isentropic exhaust blow-down through exhaust valve to constant pressure exhaust

Figure 2.2 demonstrates these processes on a typical in-cylinder pressure trace of an HCCI engine.

A simplified HCCI mathematical model is developed based on the above assumptions. In addition, the following assumptions are taken into consideration while developing the model:

a) Since natural gas is made up of 90% methane (CH_4), it is assumed that methane is the fuel used during combustion;

b) In-cylinder mixture composition is constant and obeys the ideal gas law;

c) Gases within the intake and exhaust manifolds are assumed to be at constant temperature and pressure;

d) Specific heat capacities (c_p) of fuel, air and exhaust gases, as well as their ratio of specific heat capacities (γ) are assumed constant;

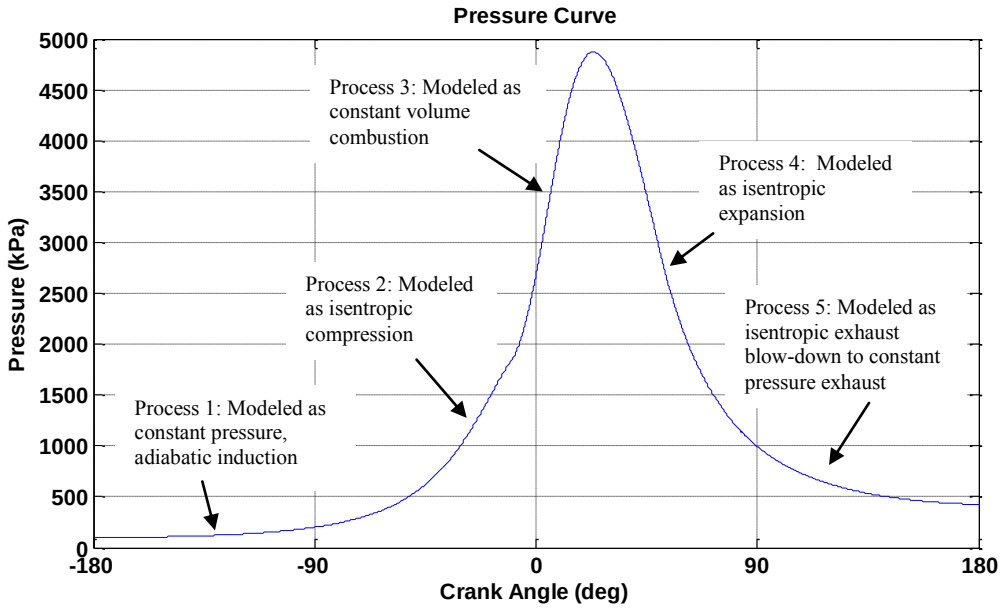

Figure 2.2 In-cylinder pressure profile showing the five thermodynamic processes of the HCCI cycle

2.2 Deriving Equations for the HCCI Thermodynamic Model

By dividing the engine cycle into five processes, it is now possible to represent each process thermodynamically. This will be the basis of the physics-based model that is going to be developed in this section while taking into account all the assumptions discussed in Section 2.1.

2.2.1 Constant Pressure, Adiabatic Induction

The first state of the engine cycle involves the induction of a lean mixture of fresh reactants (fuel and air) and EGR at constant pressure assuming no heat loss (adiabatic). Fuel is considered to be methane (CH_4) while air is assumed to be composed of oxygen (O_2) and nitrogen (N_2) with a ratio of 1:3.76 respectively. EGR is assumed to consist of carbon dioxide (CO_2), water vapor (H_2O) and nitrogen. A lean mixture means

that the equivalence ratio (φ) is less than 1. To determine the number of moles in the recirculated exhaust gases, combustion under stoichiometric conditions (φ = 1) is first considered:

$$CH_4 + 2(O_2 + 3.76N_2) \rightarrow CO_2 + 2H_2O + 7.52N_2 \quad (1)$$

Then, assuming lean conditions, Eq. (1) becomes:

$$CH_4 + \frac{2}{\varphi}(O_2 + 3.76N_2) \rightarrow CO_2 + 2H_2O + (\frac{2}{\varphi} - 2)O_2 + 3.76\left(\frac{2}{\varphi}\right)N_2 \quad (2)$$

Exhaust gases are added to the reactants side of Eq. (2) to represent EGR yielding the following final equation for the mixing process taking place during the induction:

$$\varphi_k\, CH_4 + 2(O_2 + 3.76N_2) + \alpha_k\left[\varphi_{(k-1)}\, CO_2 + 2\varphi_{(k-1)}H_2O + 2\left(1 - \varphi_{(k-1)}\right)O_2 + 7.52N_2\right]$$

$$= \varphi_k\, CH_4 + 2\left(\alpha_k\left(1-\varphi_{(k-1)}\right) + 1\right)O_2 + 7.52(1 + \alpha_k)N_2 + \varphi_{(k-1)}\alpha_k CO_2$$

$$+ 2\varphi_{(k-1)}\alpha_k H_2O \quad (3)$$

where α_k is the ratio of moles of external EGR to the moles of fresh reactants of the current kth cycle, φ_k is the equivalence ratio at the current kth cycle and $\varphi_{(k-1)}$ is the equivalence ratio at the previous cycle, k-1.

Applying the first law of thermodynamics for an open system during the induction phase results in (neglecting kinetic and potential energies):

$$\left(\frac{dU}{dt}\right)_{CV} = \dot{Q} - \dot{W} + \dot{m}_{rct}h_{rct} + \dot{m}_{EGR}h_{EGR} \quad (4)$$

where:

$\left(\frac{dU}{dt}\right)_{CV}$: Change in internal energy within the control volume, i.e. cylinder (kJ/s)

$\dot{Q}$: Change in heat transfer during the induction process (kJ/s)

$\dot{W}$: Change in work done due to piston movement, where $\dot{W} = p\dot{V}$ (kJ/s), p: pressure (kPa) and $\dot{V}$: Rate of volume change (m^3/s)

$\dot{m}_{rct}$, $\dot{m}_{EGR}$: Mass flow rates of reactants and EGR through the intake valve, respectively (kg/s).

h_{rct}, h_{EGR}: Enthalpies at intake and exhaust manifolds of the reactants and EGR, respectively (kJ/kg).

Applying the following assumptions to Eq. (4) simplifies it to Eq. (5):

1- No heat transfer during induction, $\dot{Q} = 0$

2- Constant in-cylinder pressure, $\dot{p} = 0$

3- Thermodynamical properties within the intake and exhaust manifolds are kept constant

$$\left(\frac{dU}{dt}\right)_{CV} = \dot{m}_{rct}h_{rct} + \dot{m}_{EGR}h_{EGR} \tag{5}$$

Enthalpy is related to the internal energy by the following thermodynamic equation:

$$H = U + pV \tag{6}$$

where:

H: Total enthalpy in the cylinder (kJ) and H = m*h, m: mass inside the cylinder (kg)

p: pressure (kPa) and V: volume (m^3);

By taking into consideration Eq. (6) and assumption 2 ($\dot{p} = 0$), Eq. (5) becomes:

$$\dot{m}_{EGR}h_{EGR} + \dot{m}_{rct}h_{rct} = \frac{d(mh)}{dt} \tag{7}$$

Integrating Eq. (7) while taking into consideration the third assumption mentioned above yields the following result:

$$\sum_{EGR} N_i \bar{h}_i(T_{1,\,EGR}) + \sum_{rct} N_i \bar{h}_i(T_{1,\,rct}) = \sum_{1} N_i \bar{h}_i(T_1) \tag{8}$$

where:

N_i : Number of moles of species i which can be found from Eq. (3)

$\bar{h}_i(T)$: Molar enthalpy of species i at temperature T (kJ/mol)

Specific heat capacities are considered to be constant with temperature; hence, the following approximation could be used:

$$\bar{h}_i(T) = \Delta_f \bar{h}_i + \bar{c}_{p,i}\,(T - T_{ref}) \tag{9}$$

where:

$\Delta_f \bar{h}_i$: Molar heat of formation of species i (kJ/mol)

$\bar{c}_{p,i}$: Specific heat capacity of species i (kJ/K mol)

T_{ref}: Reference temperature used to calculate $\Delta_f \bar{h}_i$ (K)

By substituting Eq. (9) into Eq. (8), the following expression for $T_{1,k}$ is obtained:

$$T_{1,k} = \frac{C_1 T_{inlet} + C_2 \alpha_k T_{prod,k}}{C_1 + C_2 \alpha_k} \tag{10}$$

where:

$$C_1 = \varphi_k \bar{c}_{p,CH_4} + 2\bar{c}_{p,O_2} + 7.52\bar{c}_{p,N_2}$$

$$C_2 = \varphi_{(k-1)}\bar{c}_{p,CO_2} + 2\varphi_{(k-1)}\bar{c}_{p,H_2O} + 2(1 - \varphi_{(k-1)})\bar{c}_{p,O_2} + 7.52\bar{c}_{p,N_2}$$

and:

$T_{1,k}$: Temperature at the end of the induction phase of the kth cycle (K)

T_{inlet}: Temperature of fresh inducted reactants (K)

$T_{prod,k}$: Temperature of external EGR (K)

Temperature of external EGR is related to the temperature of the exhaust products from the previous cycle, $T_{5,k-1}$ which is calculated at the last (fifth) stage of each engine cycle. This represents the cycle-to-cycle coupling required for the application of residual-affected control strategies. Heat losses resulting from heat transfer occurring inside the external EGR pipeline can be represented by a simplified linear relationship:

$$T_{prod,k} = \xi T_{5,k-1} \tag{11}$$

where ξ is assumed to be 0.96. This parameter was adjusted to reproduce similar data to that obtained by the GT-Power model (which will be explained in Section 2.4).

Substituting Eq. (11) into Eq. (10), the temperature at the end of the induction phase is calculated as follows:

$$T_{1,k} = \frac{C_1 T_{inlet} + C_2 \alpha_k \xi T_{5,k-1}}{C_1 + C_2 \alpha_k} \tag{12}$$

2.2.2 Isentropic Compression

Compression is occurring isentropically and the in-cylinder mixture follows the ideal gas laws. Hence, temperature and pressure at the end of compression phase and just before combustion are calculated as follows:

$$T_{2,k} = \left(\frac{V_{1,k}}{V_{SOC,k}}\right)^{\gamma-1} T_{1,k} \tag{13}$$

$$P_{2,k} = \left(\frac{V_{1,k}}{V_{SOC,k}}\right)^{\gamma} P_{1,k} \tag{14}$$

where:

$P_{1,k}$: In-cylinder pressure at intake valve closing (IVC) (kPa)

$V_{1,k}$: Volume at IVC (m^3)

$V_{SOC,k}$: Volume at the crank angle at which start of combustion occurs, θ_{SOC} (m^3)

γ: Ratio of specific heat, assumed to be 1.4

In-cylinder volume at any crank angle, θ, is calculated using the following equation:

$$V(\theta) = V_c \left[1 + \frac{1}{2}(r_c - 1)\left(R + 1 - \cos\theta - \sqrt{R^2 - \sin^2\theta}\right)\right] \quad (15)$$

where:

V_c: Clearance volume (m^3)

r_c: Compression ratio

R : $\frac{l}{a}$; where l: connecting rod length and a: crank radius

2.2.3 Constant Volume Combustion

Assuming complete combustion, the combustion reaction is as follows:

$$\varphi_{(k)}CH_4 + 2\left(\alpha_k\left(1 - \varphi_{(k-1)}\right) + 1\right)O_2 + 7.52\,(1 + \alpha_k)N_2 + \varphi_{(k-1)}\alpha_k CO_2 + 2\varphi_{(k-1)}\alpha_k H_2O$$

$$\rightarrow \left(\varphi_{(k)} + \varphi_{(k-1)}\alpha_k\right)CO_2 + 2(\varphi_{(k)} + \varphi_{(k-1)}\alpha_k)H_2O + 7.52\,(1 + \alpha_k)N_2$$

$$+ 2\left(1 + \alpha_k - \varphi_{(k)} - \varphi_{(k-1)}\alpha_k\right)O_2 \quad (16)$$

Applying the first law of thermodynamics for closed systems yields the following equation, which states:

$$\left(\frac{dU}{dt}\right)_{CV} = \dot{Q} - \dot{W} \quad (17)$$

Since combustion is occurring at constant volume, $\dot{W} = 0$. Therefore, integrating Eq. (17) results:

$$U_2 = U_3 - Q \quad (18)$$

where:

U_2: Internal energy of the mixture prior to combustion (kJ)

U_3: Internal energy of the mixture after combustion (kJ)

Q: Heat transfer during the combustion process (kJ)

According to [53], the total amount of heat transfer during the combustion process can be expressed as a percentage of the chemical energy resulting from the combustion reaction:

$$Q = LHV_{CH_4} N_{CH_4} \varepsilon \tag{19}$$

where:

LHV_{CH_4} : Lower Heating Value of CH_4 which is defined as:

$$LHV_{CH_4} = \Delta_f \bar{h}_{CO_2} + 2\Delta_f \bar{h}_{H_2O} - \Delta_f \bar{h}_{CH_4} \tag{20}$$

$\varepsilon = 0.1$, as defined in [53].

Internal energies can be re-written based on the following relation:

$$U = H - pV = H - R_u N_i T \tag{21}$$

where R_u is the Universal Gas Constant (J /K mol).

Therefore, by substituting Eq. (21) into Eq. (8), the following equations for the internal energies before and after combustion are obtained:

$$U_2 = \sum_2 N_i \bar{h}_i(T_2) - R_u T_{2,k} \sum_2 N_i$$

$$U_3 = \sum_3 N_i \bar{h}_i(T_3) - R_u T_{3,k} \sum_3 N_i \tag{22}$$

where:

$T_{2,k}$: Pre-combustion temperature (K) of the current cycle, k.

$T_{3,k}$: Post-combustion temperature (K) of the current cycle, k.

Substituting Eqs. (19) and (22) into Eq. (18) results in the following equation:

$$\sum_{2} N_i \bar{h}_i(T_2) - R_u T_{2,k} \sum_{2} N_i = \sum_{3} N_i \bar{h}_i(T_3) - R_u T_{3,k} \sum_{3} N_i + LHV_{CH_4} N_{CH_4} \varepsilon \qquad (23)$$

Rearranging Eq. (23) results in the following expression for $T_3(k)$:

$$T_{3,k} = \frac{-\sum_2 N_i \bar{h}_i(T_2) + R_u T_{2,k} \sum_2 N_i + \sum_3 N_i \bar{h}_i(T_3) + LHV_{CH_4} N_{CH_4} \varepsilon}{R_u \sum_3 N_i} \qquad (24)$$

After substituting the respective N_i terms from Eq. (16) and using the relation in Eq. (9), $T_3(k)$ is found by:

$$T_{3,k} = \frac{C_3 + T_{2,k}[C_1 + \alpha_k C_2 - C_4]}{C_5 + \alpha_k C_2 - C_4} \qquad (25)$$

where:

$$C_4 = Ru\ (\varphi_{(k-1)} + 9.52\alpha_k + \alpha_k\ \varphi_{(k-1)} + 9.52)$$

$$C_5 = \varphi_k \bar{c}_{p,CO_2} + 2\varphi_k \bar{c}_{p,H_2O} + 2(1 - \varphi_k)\bar{c}_{p,O_2} + 7.52\bar{c}_{p,N_2}$$

$$C_3 = LHV_{CH_4}\ \varphi_k(1 - \varepsilon) - (C_5 - C_1)\ T_{ref}$$

Using the ideal gas relation and assuming constant volume, post-combustion pressure, P_3, is calculated by:

$$P_{3,k} = \frac{\sum_3 N_i}{\sum_2 N_i} P_{2,k} \frac{T_{3,k}}{T_{2,k}} \qquad (26)$$

Substituting Eqs. (13), (14) and (25) into Eq. (26), results in the following expression for post-combustion in-cylinder pressure (peak pressure):

$$P_{3,k} = \frac{\sum_3 N_i}{\sum_2 N_i} \left(\frac{V_{1,k}}{V_{SOC,k}} \right)^{\gamma} \frac{C_1 + \alpha_k C_2 - C_4}{T_{3,k}[C_5 + \alpha_k C_2 - C_4] - C_3} P_{1,k} T_{3,k} \qquad (27)$$

2.2.4 Isentropic Expansion

Isentropic expansion is the fourth stage in the engine cycle where the gas expands isentropically until EVO. Using ideal gas equation, temperature and pressure at EVO, T_4 and P_4, respectively, can be written as functions of post-combustion temperature, T_3, and post-combustion pressure, P_3:

$$T_{4,k}= \left(\frac{V_{SOC,k}}{V_{4,k}}\right)^{\gamma-1} T_{3,k} \tag{28}$$

$$P_{4,k}= \left(\frac{V_{SOC,k}}{V_{4,k}}\right)^{\gamma} P_{3,k} \tag{29}$$

2.2.5 Isentropic Exhaust Blow-Down to Constant Pressure Exhaust

The final stage is the exhaust blow-down to atmospheric pressure, through the exhaust valve, which is also assumed to occur isentropically. In addition, the exhaust process which occurs from EVO until intake valve opening (IVO) is assumed to occur at constant pressure, i.e. atmospheric pressure, and adiabatically. Assuming ideal exhaust blow-down, the exhaust temperature, T_5, which is also the temperature at exhaust blow-down can be expressed as:

$$T_{5,k} = \left(\frac{P_{atm}}{P_{4,k}}\right)^{\frac{\gamma-1}{\gamma}} T_{4,k} \tag{30}$$

2.3 Modeling Ignition Timing

After developing the HCCI model based on the assumptions made in Section 2.1, the onset of combustion, θ_{SOC}, has to be modeled to determine the volume at SOC, V_{SOC}, which is needed in several of the equations in Section 2.2. Several approaches have been

mentioned previously in Section 1; however the two most common correlations used are the Arrhenius Rate Integral [24] and the Modified Knock Integral Model (MKIM) [54].

In reality, the combustion process consists of several sub-reactions to transform the reactants to exhaust products. The chemical kinetics models mentioned in Section 1.3.1 attempt to model these reactions. However, due to the computation time and complexity of these chemical equations, such models cannot be used for control purposes. Instead, a single global reaction rate expression has been used in an attempt to simplify modeling the combustion process. The reaction rate is known as the Arrhenius Reaction Rate Equation, developed by Svante Arrhenius in 1889 [55] and takes the following form:

$$k_R = A \exp\left(-\frac{E_a}{RT}\right) \tag{31}$$

where:

E_a: Activation energy of the fuel (kJ/mol)

R_u: Universal Gas Constant (J/K mol)

A: Arrhenius rate pre-exponential factor (sec^{-1} for a first order reaction, $dm^3\ mol^{-1}\ sec^{-1}$ for a second order reaction)

T: Temperature of mixture (K)

A and E_a/R_u are empirical parameters that are determined using combustion kinetic experiments.

As shown in Eq. (31), the Arrhenius equation correlates the effect of temperature to the reaction rate. Many other correlations were based on the Arrhenius rate equation

[56-59], however the most common is the Integrated Arrhenius Reaction Rate which was used in [24] and is of the following form:

$$\int RR = \int_{\theta_{IVC}}^{\theta_{th}} \frac{A_{th} e^{(\frac{E_a}{R_u T})} [fuel]^a [O_2]^b}{\omega} d\theta = K_{th} \quad (32)$$

where:

θ_{th}: crank angle at which start of combustion occurs (deg)

θ_{IVC}: crank angle at which IVC occurs (deg)

A_{th}: Arrhenius rate pre-exponential factor ((gmol/cm^3)$^{1-a-b}$/sec)

T: instantaneous in-cylinder temperature (K)

ω: engine speed (rad/sec)

and:

$$[fuel] = \frac{n_{fuel,k}}{V}$$

$$[O_2] = \frac{n_{O_2,k}}{V}$$

$n_{fuel,k}$: instantaneous number of moles of fuel inside cylinder at engine cycle, k

$n_{O_2,k}$: instantaneous number of moles of oxygen inside cylinder at engine cycle, k

V: instantaneous volume inside cylinder at engine cycle, k (m^3)

A_{th}, E_a/R_u, a and b are empirical parameters that are determined using combustion kinetic experiments.

The integrated Arrhenius reaction rate involves integrating the Arrhenius expression and determines the reaction rate in terms of temperature, fuel and oxygen

concentrations, as well as engine speed. Since temperature and species concentration are the two main parameters that effect HCCI combustion, this correlation can be used to model the start of combustion in HCCI engines.

The MKIM correlation is a modified version of the Knock Integral Model (KIM). The original knock integral method [60] was initially developed to investigate the "knocking" effect in spark-ignition engines. Engine knock occurs when the fuel and air mixture ignites prematurely inside the cylinder causing noise and damage to the engine. Since HCCI combustion depends on the auto-ignition of a homogeneous charge of fuel and air mixture, then using the knock integral method seems as a good start. Using the same theory behind the knock integral method, Livengood et al. [60] developed a correlation that would predict when a homogeneous mixture of fuel and air would auto-ignite, which was later known to be the KIM. This model depended on the time interval needed to ignite a fuel-air mixture defined as a function of pressure, temperature and chemical composition. If the physical state of the mixture is assumed to be constant, this time interval is known as the ignition delay, τ:

$$\tau = A \exp\left(\left(\frac{b}{T}\right) P^n \right) \tag{33}$$

where:

τ: ignition delay time (sec)

T: temperature of mixture as a function of crank angle (K)

P: pressure of mixture as a function of crank angle (kPa)

A, b and n are empirical constants to be determined experimentally.

Furthermore, when time is replaced by crank angle through using the engine speed, the ignition correlation becomes the following:

$$\int_{\theta_{IVC}}^{\theta_{knock}} \frac{1}{\omega\tau}\, d\theta = \int_{\theta_{IVC}}^{\theta_{knock}} \frac{1}{\omega A\, e^{(b/T)P^n}}\, d\theta = 1 \qquad (34)$$

where:

θ_{knock}: the crank angle at which knock occurs

θ_{IVC}: crank angle at which intake valve closes (IVC)

ω: engine speed (revolutions per minute, RPM)

Therefore, when the value of the integrand reaches 1, auto-ignition occurs at $\theta = \theta_{knock}$.

Swan et al. [54] proposed the modified version of the KIM, MKIM, so that the correlation could be used for HCCI engines rather than spark-ignition engines. By adding a few terms such as fuel concentration, oxygen concentration and EGR rate, the correlation became more dependent on chemical kinetics. The compression process is assumed to be polytropic (PV^n = constant), which dictates the relationship between pressure and volume if n is assumed to be constant. Swan believed this was a practical assumption instead of determining the actual relationship between pressure and volume from experimental data. This is because most commercial engines are not equipped with pressure and temperature sensors to obtain instantaneous pressure and temperature data. Fuel and oxygen concentrations are replaced by the equivalence ratio which is a good indication of the amount of air and fuel present. This also simplifies the model and avoids the need to find instantaneous fuel and oxygen concentrations which can be

practically challenging. After adding these simplifications, the MKIM [54] correlation becomes:

$$\int_{\theta_{IVC}}^{\theta_{SOC}} \frac{1}{A\omega \exp\left(\frac{b\left(P_{IVC}v_c^{n_c}\right)^n}{T_{IVC}v_c^{n_c-1}}\right)} \varphi^x \, d\theta = 1 \qquad (35)$$

where:

θ_{SOC}: crank angle at which Start of Combustion (SOC) occurs (deg)

P_{IVC}: pressure at IVC at engine cycle, k (kPa)

T_{IVC}: temperature at IVC at engine cycle, k (K)

φ: equivalence ratio

n_c: polytropic parameter (ratio of specific heat) of the mixture, which is considered to be constant

ω: engine speed (rad/sec)

and:

$$v_c = \frac{V(\theta_{IVC})}{V(\theta)}$$

$V(\theta_{IVC})$: volume at IVC (m^3)

$V(\theta)$: instantaneous in-cylinder volume (m^3)

A, b, n and x are empirical parameters obtained though experimental data.

After thoroughly comparing both correlations, the MKIM correlation is chosen to model the start of combustion. One of the major advantages that MKIM has over the Integrated Arrhenius Rate is that the former will not require determining molar

concentrations of fuel and oxygen which would be experimentally challenging to achieve. In addition, model validation (Section 2.4) will be performed via a single-cylinder engine model that was designed using GT-Power [61], a powerful engine simulation tool developed by Gamma Technologies. One of the correlations that GT-Power uses is KIM which is closely related to MKIM, making it a better option for ignition timing validation than the Arrhenius expression.

To be able to use MKIM, the empirical parameters A, b, n and x need to be determined experimentally. In order to optimize the parameters to fit the data, the error in the integral needs to be minimized so that it reaches 1. Numerical minimization is done using a MATLAB function which is based on the Nelder-Mead simplex minimization method [62]. A MATLAB code is developed to optimize the parameters and then substitutes them back into the MKIM integrand (Eq. (35)). θ_{SOC} is assumed to occur within a range of values. Integration is then performed by substituting a value for θ_{SOC} within the specified range until the integration equals 1. Hence, that value of θ_{SOC} is considered the crank angle at which ignition occurs. Table 2.1 shows the optimized values for the empirical parameters that were achieved using the above method.

Table 2.1 Values for MKIM model parameters

Parameter	Value
A	$(1.3109*EGR + 13.325) * 10^{-4}$
b	11398
n	-0.4218
x	-1.5144

(Note: EGR value represents the percentage of EGR of the inducted mixture)

2.4 Validation of the Physics-Based Model

As mentioned in Section 2.3, results obtained from the HCCI thermodynamic model was validated using a single-cylinder engine model developed using GT-Power (Figure 2.3) [61]. The engine operating conditions are shown in Table 2.2.

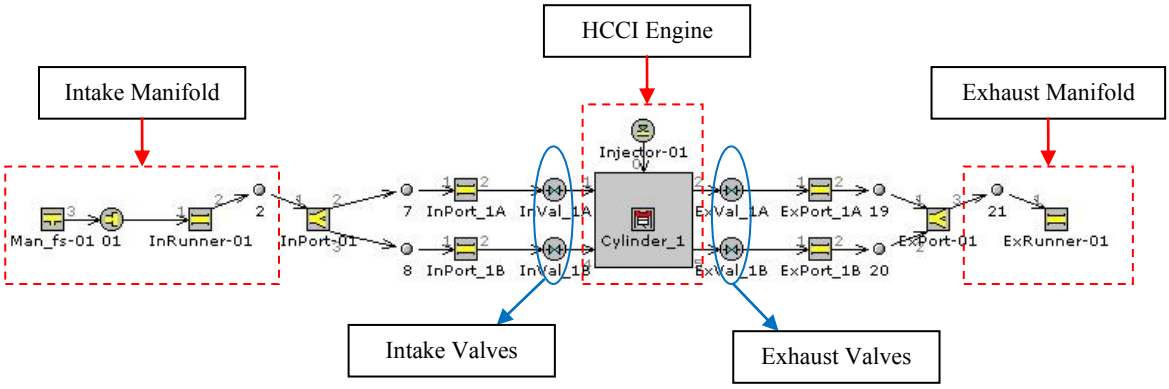

Figure 2.3 HCCI model produced by GT Power

Table 2.2 Engine operating conditions

Engine Speed	1000	RPM
Stroke	75	mm
Bore	86	mm
Connecting Rod Length	119	mm
Compression Ratio	21.5	-
Intake Valve Closure (IVC)	209	rad
Exhaust Valve Opening (EVO)	486	rad
Equivalence Ratio	0.5	-

Figures 2.4 and 2.6 show results obtained using GT-Power [61] where two ignition timing correlations were used, KIM and the third derivative of pressure with respect to crank angle degrees (CAD). The third derivative of pressure is another way to

compute ignition timing and it is calculated using Chemkin, a software tool used to solve chemical kinetic equations. Figure 2.4 shows how ignition timing varies when temperature and pressure at IVC changes. As expected, ignition timing advances as temperature and pressure at IVC increases. An increased temperature at IVC means the mixture temperature has increased causing ignition to occur earlier in the engine cycle. Increasing pressure at IVC causes ignition timing to advance because the overall mixture pressure has been increased. Figure 2.6 shows how ignition timing changes with varying temperature at IVC and EGR ratios. In this case however, as the EGR ratio increases, ignition timing is delayed. This is because EGR introduces exhaust gases such as CO_2, H_2O and O_2 into the cylinder which are inert species that do not contribute to the combustion. In fact, they absorb thermal energy since they need to be heated along with the other species and therefore act as "energy absorbers". By increasing the amount of EGR in the cylinder, more "energy absorbers" are available. This results in a decrease in the mixture temperature, hence causing combustion to occur at a later time. The same data at the same operating conditions were reproduced using the MKIM correlation with the optimized parameters in Table 2.1. A code was written in MATLAB to calculate the integral and plot the results, as shown in Figures 2.5 and 2.7.

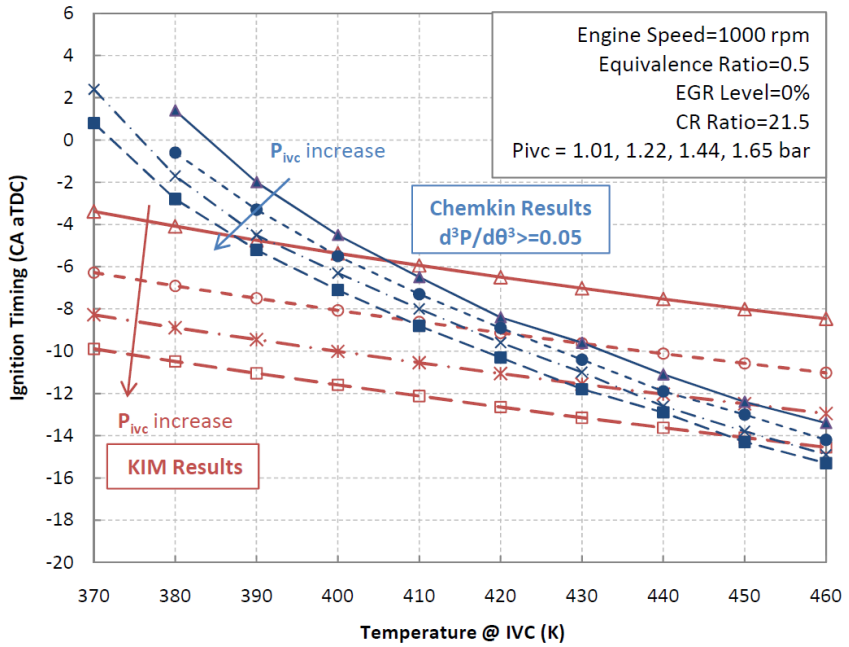

Figure 2.4 Effect of intake pressure on ignition timing of natural gas under HCCI conditions using GT Power

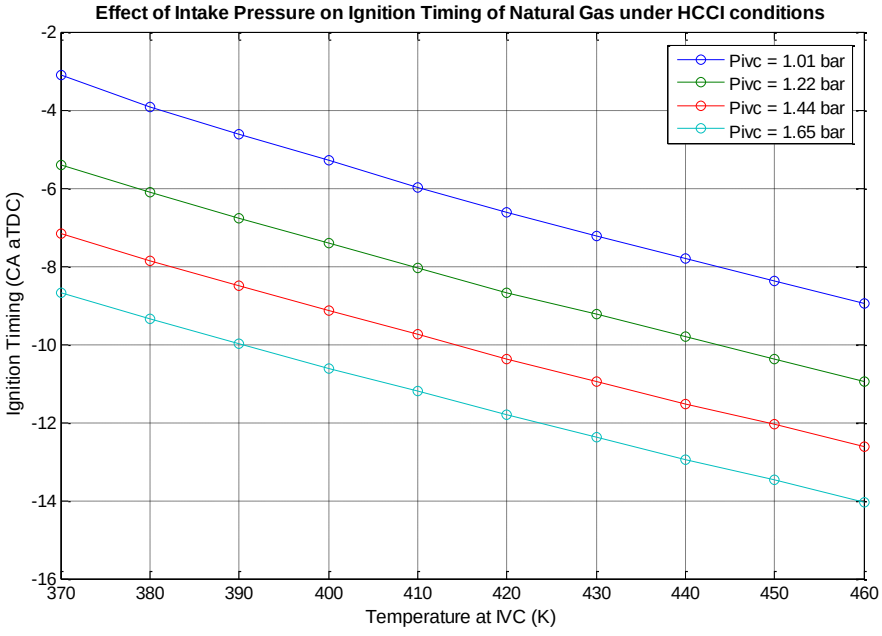

Figure 2.5 Effect of intake pressure on ignition timing of natural gas under HCCI conditions using MKIM correlation

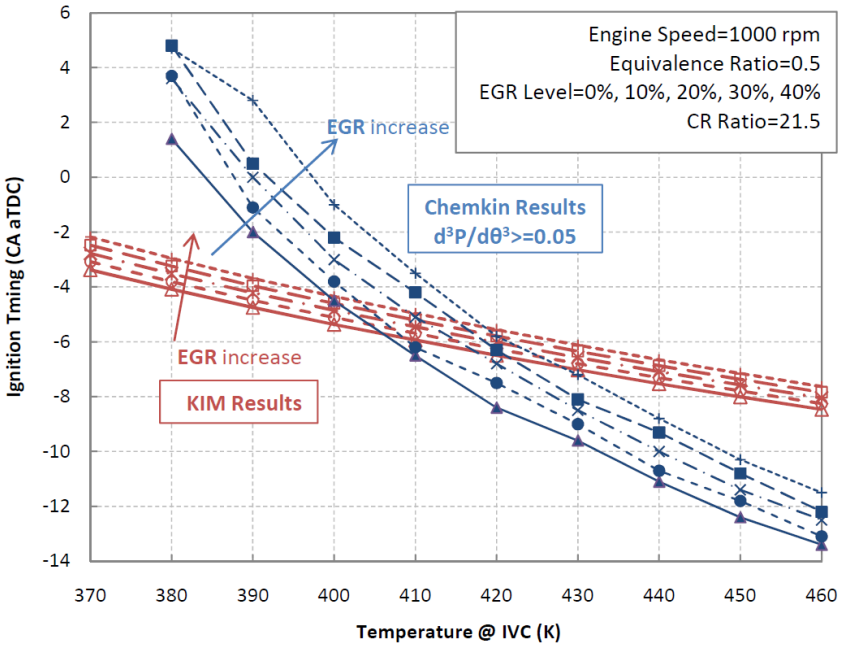

Figure 2.6 Effect of EGR on ignition timing of natural gas under HCCI conditions using GT Power

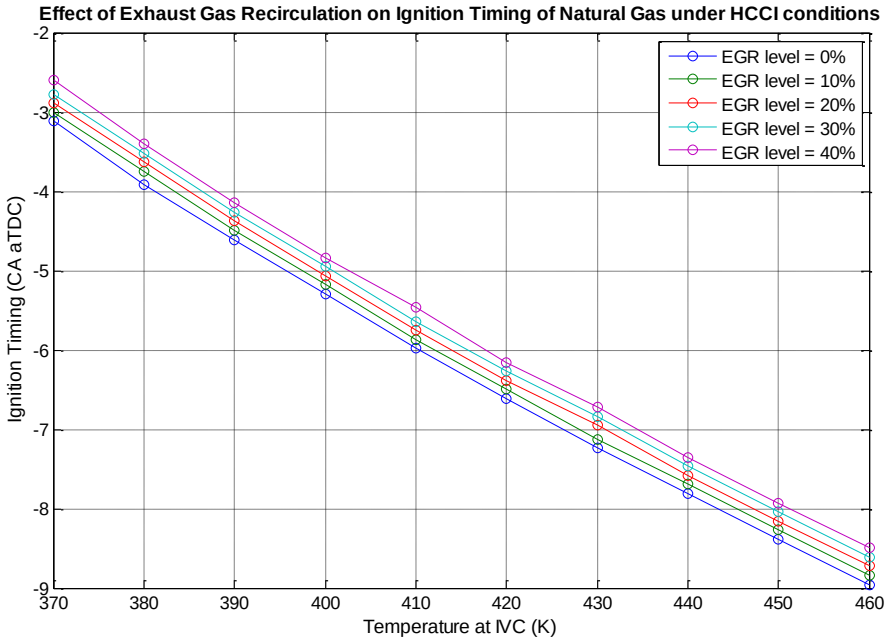

Figure 2.7 Effect of EGR on ignition timing of natural gas under HCCI conditions using MKIM correlation

Results in Figure 2.5 were compared to those generated by the KIM model in Figure 2.4 and results in Figure 2.7 were compared to those produced by the KIM model in Figure 2.6. By comparing the above figures, it was verified that the values of the empirical parameters in Table 2.1 obtained through optimization, resulted in data that was in close correlation with data from GT Power. Hence, these values can be used to predict start of combustion within the proposed HCCI thermodynamic model.

2.5 Conclusions

In order to model an HCCI engine fuelled by natural gas, a physics-based model was developed to model the thermodynamics of the engine. The engine cycle was divided into five processes and each was represented thermodynamically using the first law of thermodynamics, as well as ideal gas laws. To model ignition timing, both the Arrhenius rate integral and the MKIM were studied and compared to choose the model which best suits the application and would not be experimentally challenging. The MKIM was found to be the best option.

A MATLAB code was developed which used a least-squares minimization error function to determine the empirical parameters used in the MKIM correlation. The MKIM correlation was evaluated using another MATLAB code and ignition timing was determined by varying inlet temperature, intake pressure and EGR ratio. Validation was performed using data produced by an engine model developed by GT-Power. The model was able to reproduce similar results to GT-Power.

In the next section, a nonlinear control model will be developed based on the physics-based model developed in this section.

3. DEVELOPMENT OF THE NONLINEAR MODEL AND ITS LINEARIZATION

In this section, a closed-loop control model is designed to control the ignition timing of HCCI engines. Since lack of a direct combustion trigger is one of the main drawbacks to HCCI implementation, the development of an indirect method is necessary to control the ignition timing. The percentage of exhaust gases re-inducted back into the cylinder, α_k, will serve as the control input, while temperature at intake valve closure (IVC), $T_{IVC,k-1}$, will be the control output. The thermodynamic model developed in Section 2 provides the foundation for determining the relationships between control variables, α_k and $T_{IVC,k-1}$.

3.1 Defining Model Variables

Combustion timing is usually controlled to ensure maximum efficiency, while maintaining low emission levels. In this research, Exhaust Gas Recirculation (EGR) ratio, α_k, will be considered as the input to control combustion timing. By adjusting α_k, the temperature and chemical composition of the homogeneous fuel-air mixture inside the cylinder will be altered and hence indirectly controlling the auto-ignition timing of the mixture. Figure 2.5 showed how an increase in EGR ratio led to a delay in combustion timing, confirming that α_k can be used as a proper control input variable.

Regarding the output control variable, the crank angle at which start of combustion occurred (θ_{SOC}) was initially considered as an option. However, it was found that to successfully implement this output variable, the MKIM correlation (Eq. (35)) that

is used to predict start of combustion will have to be linearized since a linear control system will be applied to the nonlinear model. Linearizing an integral was found to be quite a challenging task. Therefore temperature at IVC, T_{IVC}, is chosen as the control output variable since the relationship between T_{IVC} and the input, α_k, i.e. Eq. (12) is easier to linearize. The MKIM correlation is used to determine the value of T_{IVC} causing combustion to occur at a required crank angle. Hence, the control system develops into adjusting α_k, by changing the position of the EGR valve, to achieve the required T_{IVC}.

To determine the value of T_{IVC} that will cause combustion to take place at a desired set point, a relationship between θ_{SOC} , crank angle at which start of combustion (SOC) occurs, and T_{IVC} is needed. Considering the Modified Knock Integral Model (MKIM) correlation in Eq. (35) used to predict ignition timing, it is noticeable that if P_{IVC}, ω, φ and n_c are kept constant, then a direct relationship between T_{IVC} and θ_{SOC} is achieved.

$$\int_{\theta_{IVC}}^{\theta_{SOC}} \frac{1}{A\omega \exp\left(\frac{b\left(P_{IVC}v_c^{n_c}\right)^n}{T_{IVC}v_c^{n_c-1}}\right)} \varphi^x \, d\theta = 1 \qquad (35)$$

The desired ignition timing, θ_{des} is substituted with the value of θ_{SOC} in the above integral while T_{IVC} is assumed to take on a range of values (300 – 450 K). The integrand is evaluated at each value of T_{IVC}. Once the integration yields the value of 1, then the corresponding value of T_{IVC} is used as the desired temperature needed to be achieved by changing α_k. Figure 3.1 shows a flowchart explaining the above procedure of how the

EGR ratio will be used to influence T_{IVC} to start combustion at a desired crank angle, θ_{des}.

In order to use state-space control methods, certain "states" must be defined that can completely describe the dynamics of the system. Since exhaust gases from the previous cycle affects the properties of the mixture at the current cycle, a set of variables is needed to represent this relationship. Therefore, the states of the model were chosen to be α_{k-1}, the previous value of the input state, α_k, and $T_{IVC,\,k-1}$, same as the output. The selection of these states ensures the consideration of cycle-to-cycle coupling when studying transient response.

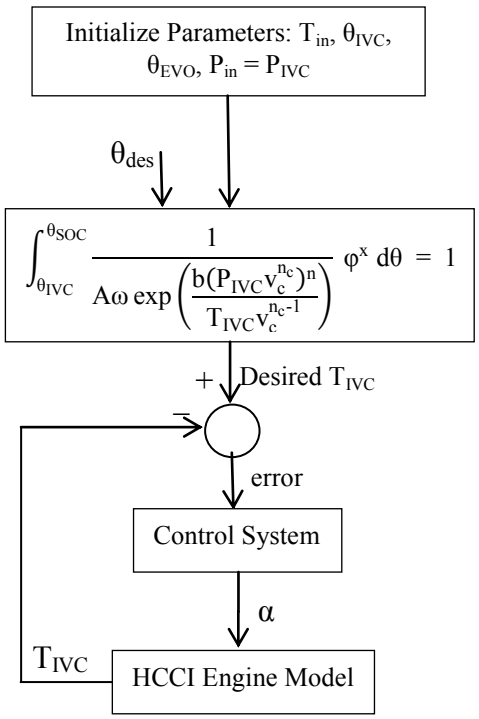

Figure 3.1 Flowchart showing the development of the control model

3.2 Nonlinear Relationship between Input and Output

Before starting to develop a controller, a relationship between the control input, α_k, and output, $T_{IVC,k-1}$, is required in terms of the state variables, α_{k-1} and $T_{IVC,\,k-1}$. The following relationship can be found through Eq. (12) of the HCCI physics-based thermodynamic model:

$$T_{1,k} = \frac{C_1 T_{inlet} + C_2 \alpha_k \xi T_{5,k-1}}{C_1 + C_2 \alpha_k} \tag{12}$$

As shown above, $T_{1,k}$ which is T_{IVC} of the current cycle ($T_{IVC,\,k}$), is in terms of α_k, the control input. It is also in terms of $T_{5,k-1}$ which represents the temperature of the re-inducted exhaust gases from the previous state. $T_{5,k-1}$ can be expressed in terms of the previous state variables, α_{k-1} and $T_{IVC,k-1}$, using the thermodynamic equations, Eqs. (12), (13), (14), (25), (27) – (30), used in the model developed in Section 2. This can be achieved by substituting each thermodynamic stage with the equation relating it to the previous stage, but making sure to use values from the previous cycle, i.e. use k-1 instead of k. For example, Eq. (30) can be used to express $T_{5,k-1}$ in terms of $T_{4,k-1}$, hence the new relationship becomes:

$$T_{5,k-1} = \left(\frac{P_{atm}}{P_{4,k-1}}\right)^{\frac{\gamma-1}{\gamma}} T_{4,k-1} \tag{36}$$

In a similar manner, $T_{4,k-1}$ can be expressed in terms of $T_{3,k-1}$ using Eq. (28) while substituting values from the previous engine cycle. By substituting Eq. (28) into Eq. (36), $T_{5,k-1}$ is now expressed in terms of $T_{3,k-1}$:

$$T_{5,k-1} = \left(\frac{P_{atm}}{P_{4,k-1}}\right)^{\frac{\gamma-1}{\gamma}} \left(\frac{V_{SOC,k-1}}{V_{4,k-1}}\right)^{\gamma-1} T_{3,k-1} \tag{37}$$

The only variables in Eq. (37) that need to be expressed in terms of state variables are $P_{4,k-1}$ and $T_{3,k-1}$ since the rest of the variables are considered constant. Eq. (29) is substituted into Eq. (37) to eliminate all variables from the previous thermodynamic state, i.e. state 4:

$$T_{5,k-1} = \left(\frac{P_{atm}}{P_{3,k-1}}\right)^{\frac{\gamma-1}{\gamma}} T_{3,k-1} \tag{38}$$

By following the same procedure and using Eqs. (13), (14), (25) and (26), T_5 can be expressed in terms of the first thermodynamic state, T_1, and therefore in terms of the model state variables:

$$T_{5,k-1} = \frac{P_{atm}^{\frac{\gamma-1}{\gamma}}}{\left(\frac{\sum_3 N_i}{\sum_2 N_i}\right)} \left(\frac{V_1 P_{atm}}{V_{SOC} T_{IVC,k-1}}\right)^{\frac{1-\gamma}{\gamma}} \left(\frac{c_3 + \left(\frac{V_1}{V_{SOC}}\right)^{\gamma-1} (c_1 + c_2\alpha_{k-1} - c_4) T_{IVC,k-1}}{c_5 + c_2\alpha_{k-1} - c_4}\right)^{\frac{1}{\gamma}} \tag{39}$$

For simplicity, the total number of moles after combustion, ΣN_3 can be approximated as the total number of moles prior to combustion, ΣN_2. Hence, Eq. (39) simplifies to:

$$T_{5,k-1} = P_{atm}^{\frac{\gamma-1}{\gamma}} \left(\frac{V_1 P_{atm}}{V_{SOC} T_{IVC,k-1}}\right)^{\frac{1-\gamma}{\gamma}} \left(\frac{c_3 + \left(\frac{V_1}{V_{SOC}}\right)^{\gamma-1} (c_1 + c_2\alpha_{k-1} - c_4) T_{IVC,k-1}}{c_5 + c_2\alpha_{k-1} - c_4}\right)^{\frac{1}{\gamma}} \tag{40}$$

As shown in Eq. (40), $T_{5,k-1}$ is now expressed in terms of constants (P_{atm}, γ, V_{SOC}, V_1, c_1, c_2, c_3, c_4 and c_5) and model state variables (α_{k-1} and $T_{IVC,\,k-1}$). The final step is to

substitute Eq. (40) back into Eq. (12) in order to obtain the final input-output relationship, Eq. (41), that will be used to develop the controller.

$$T_{IVC,k}=$$

$$\frac{c_1 T_{in,k}+ c_2\alpha_k}{c_1+ c_2\alpha_k}\left[P_{atm}^{\frac{\gamma-1}{\gamma}}\left(\frac{V_1 P_{atm}}{V_{SOC}T_{IVC,k-1}}\right)^{\frac{1-\gamma}{\gamma}}\left(\frac{c_3+\left(\frac{V_1}{V_{SOC}}\right)^{\gamma-1}(c_1+ c_2\alpha_{k-1}- c_4)T_{IVC,k-1}}{c_5 + c_2\alpha_{k-1}-c_4}\right)^{\frac{1}{\gamma}}\right] \quad (41)$$

Eq. (41) shows that the relationship between the input and output is highly nonlinear which is expected since the equation was derived using nonlinear thermodynamical laws and ideal gas equations.

3.3 Linearization of the Input – Output Relationship

The design of many control strategies is based on a linear model. Consequently, the nonlinear input-output relationship, Eq. (41) has to be linearized.

A perturbation method is used to linearize Eq. (41) similar to that used in [48] which involves linearizing temperature at IVC about a certain operating point ($\overline{\alpha_k}$, $\overline{T_{IVC,k}}$, $\overline{\alpha_{k-1}}$, $\overline{T_{IVC,k-1}}$). Linear expansions for the input, output and state variables results in the following:

$$T_{IVC,k}= \overline{T_{IVC,k}}+\widetilde{T_{IVC,k}} \quad (42)$$

$$\alpha_k= \overline{\alpha_k}+\widetilde{\alpha_k} \quad (43)$$

$$T_{IVC,k-1}= \overline{T_{IVC,k-1}}+\widetilde{T_{IVC,k-1}} \quad (44)$$

$$\alpha_{k-1}= \overline{\alpha_{k-1}}+\widetilde{\alpha_{k-1}} \quad (45)$$

where $\widetilde{\alpha_k}$, $\widetilde{T_{IVC,k}}$, $\widetilde{T_{IVC,k-1}}$, $\widetilde{\alpha_{k-1}}$ are infinitesimal fluctuation terms of the state variables.

The perturbation method suffers from a major drawback: it has to be applied to a nonlinear first order equation. In Eq. (41) some of the model variables are raised to a non-integer power that cannot be expanded to first-order terms. To solve this problem, binomial expansion is applied where the first three terms of the expanded expression are used that result in errors less than 5%. Eq. (41) was first simplified into Eq. (46) by grouping some terms and defining new constants to facilitate the expansion and linearization process:

$$T_{IVC,k} = \frac{c_1 T_{in,k}}{c_1 + c_2 \alpha_k} + \frac{c_2 \alpha_k c_6^{1-\gamma/\gamma}}{c_1 + c_2 \alpha_k} \left[\left(\frac{1}{T_{IVC,k-1}} \right)^{1-\gamma/\gamma} \left(\frac{1}{c_9 + c_2 \alpha_{k-1}} \right)^{\frac{1}{\gamma}} (c_3 + c_7 T_{IVC,k-1} + c_8 \alpha_{k-1} T_{IVC,k-1})^{\frac{1}{\gamma}} \right] \quad (46)$$

where:

$$c_6 = \frac{V_{1,k-1}}{V_{SOC,k-1}}$$

$$c_7 = \left(\frac{V_{1,k-1}}{V_{SOC,k-1}} \right)^{\gamma-1} (c_1 - c_4)$$

$$c_8 = \left(\frac{V_{1,k-1}}{V_{SOC,k-1}} \right)^{\gamma-1} c_2$$

$$c_9 = c_5 - c_4$$

$$n = \frac{1}{\gamma}$$

$$c_{10} = \frac{1 - \gamma}{2\gamma^2}$$

$$n - 1 = \frac{1 - \gamma}{\gamma}$$

Applying binomial expansion to the three terms inside the bracket, as well as defining new constants, transforms Eq. (46) into the nonlinear Eq. (47).

$$T_{IVC,k}(c_1+c_2\alpha_k) = c_1 T_{in,k} + \beta_{19}\alpha_k \begin{bmatrix} T_{IVC,k-1}{}^{1-n}\left(\beta_1 - \beta_2\alpha_{k-1} - \beta_3\alpha_{k-1}{}^2\right) \\ + T_{IVC,k-1}{}^{2-n}\left(\beta_4+\xi_1\alpha_{k-1}+\xi_2\alpha_{k-1}{}^2-\beta_9\alpha_{k-1}{}^3\right) \\ +T_{IVC,k-1}{}^{3-n}(\beta_{10}+ \xi_3\alpha_{k-1}+\xi_4\alpha_{k-1}{}^2+\xi_5\alpha_{k-1}{}^3-\beta_{18}\alpha_{k-1}{}^4 \end{bmatrix} \quad (47)$$

where:

$$\beta_1 = \left(\frac{c_3}{c_9}\right)^n, \quad \beta_2 = \frac{nc_3{}^n c_2}{c_9{}^{n+1}}, \quad \beta_3 = \frac{n(-n-1)c_3{}^n c_2{}^2}{2c_9{}^{n+2}}$$

$$\beta_4 = \frac{nc_3{}^{n-1}c_7}{c_9{}^n}, \quad \beta_5 = \frac{n^2c_3{}^{n-1}c_7c_2}{c_9{}^{n+1}}, \quad \beta_6 = \frac{n^2(-n-1)c_3{}^{n-1}c_7c_2{}^2}{2c_9{}^{n+2}}$$

$$\beta_7 = \frac{nc_3{}^{n-1}c_8}{c_9{}^n}, \quad \beta_8 = \frac{n^2c_3{}^{n-1}c_8c_2}{c_9{}^{n+1}}, \quad \beta_9 = \frac{n^2(-n-1)c_3{}^{n-1}c_8c_2{}^2}{2c_9{}^{n+2}}$$

$$\beta_{10} = \frac{c_{10}c_3{}^{n-2}c_7{}^2}{c_9{}^n}, \quad \beta_{11} = \frac{nc_{10}c_3{}^{n-2}c_7{}^2c_2}{c_9{}^{n+1}}, \quad \beta_{12} = \frac{n(-n-1)c_{10}c_3{}^{n-2}c_7{}^2c_2{}^2}{2c_9{}^{n+2}}$$

$$\beta_{13} = \frac{2c_{10}c_3{}^{n-2}c_7c_8}{c_9{}^n}, \quad \beta_{14} = \frac{2nc_{10}c_3{}^{n-2}c_7c_8c_2}{c_9{}^{n+1}}, \quad \beta_{15} = \frac{n(-n-1)c_{10}c_3{}^{n-2}c_7c_8c_2{}^2}{c_9{}^{n+2}}$$

$$\beta_{16} = \frac{c_{10}\,c_3{}^{n-2}c_8{}^2}{c_9{}^n}, \quad \beta_{17} = \frac{nc_{10}\,c_3{}^{n-2}c_8{}^2c_2}{c_9{}^{n+1}}, \quad \beta_{18} = \frac{n(-n-1)c_{10}c_3{}^{n-2}c_8{}^2c_2{}^2}{2c_9{}^{n+2}}$$

$$\beta_{19} = c_2c_6{}^{n-1} = c_2c_6{}^{\frac{1-\gamma}{\gamma}}$$

$$\left(\frac{1}{T_{IVC,k-1}}\right)^{\frac{1-\gamma}{\gamma}} = \left(\frac{1}{T_{IVC,k-1}}\right)^{n-1} = T_{IVC,k-1}{}^{1-n}$$

$$\beta_{20}=(1-n)\beta_{19}T_{IVC,k-1}{}^{-n}, \quad \beta_{21}=(2-n)\beta_{19}T_{IVC,k-1}{}^{1-n}, \quad \beta_{22}=(3-n)\beta_{19}T_{IVC,k-1}{}^{2-n}$$

and:

$$\xi_1=-\beta_5+\beta_7, \quad \xi_2=-\beta_6-\beta_8, \quad \xi_3=-\beta_{11}+\beta_{13}, \quad \xi_4=-\beta_{12}-\beta_{14}+\beta_{16}, \quad \xi_5=-\beta_{15}-\beta_{17}$$

Although this equation still contains model parameters that are not of the first order, the powers are integers that can now be expanded easily. The only exception is $T_{IVC,\,k-1}$ with powers of (1- n), (2-n), and (3-n) that will be expanded one more time using binomial expansion but after applying the perturbation method. This simplifies the process and will be explained in further detail shortly.

The nonlinear input-output expression is now ready to be linearized using the perturbation method. All input, output and state variables in Eq. (47) will be substituted by their linear expansions (Eqs, (42)-(45)) and second, third, and fourth-order fluctuations terms will be ignored due to their infinitesimal values, i.e. ($\widetilde{\alpha_k}\widetilde{\alpha_k}$, $\widetilde{T_{IVC,k}}\widetilde{T_{IVC,k}}$, $\widetilde{\alpha_k}\widetilde{T_{IVC,k}}$, $\widetilde{\alpha_k}\widetilde{\alpha_k}\widetilde{\alpha_{k-1}}$, $\widetilde{\alpha_k}\widetilde{T_{IVC,k}}\widetilde{T_{IVC,k}}\widetilde{T_{IVC,k-1}}$, etc.). To address the problem of the $T_{IVC,\,k-1}$ terms with non-integer powers, linear expansions of $T_{IVC,\,k-1}$, Eq. (44), are first substituted to reach the following expressions:

$$\left(\overline{T_{IVC,k}}+\widetilde{T_{IVC,k}}\right)^{1-n},$$

$$\left(\overline{T_{IVC,k}}+\widetilde{T_{IVC,k}}\right)^{2-n},$$

$$\text{and } \left(\overline{T_{IVC,k}}+\widetilde{T_{IVC,k}}\right)^{3-n}$$

Applying the binomial expansion to the first equation, for example, while taking into consideration only the first three terms as before, yields the following:

$$\left(\overline{T_{IVC,k-1}}+\widetilde{T_{IVC,k-1}}\right)^{1-n}=\overline{T_{IVC,k-1}}^{1-n}+(1-n)\overline{T_{IVC,k-1}}^{-n}\widetilde{T_{IVC,k-1}}+\frac{(1-n)(-n)}{2}\overline{T_{IVC,k-1}}^{-n-1}\widetilde{T_{IVC,k-1}}^{2}$$

The second-order fluctuation term is ignored as per the perturbation method. Therefore, the final equation becomes:

$$\left(\overline{T_{IVC,k-1}}+\widetilde{T_{IVC,k-1}}\right)^{1-n}=\overline{T_{IVC,k-1}}^{1-n}+(1-n)\overline{T_{IVC,k-1}}^{-n}\widetilde{T_{IVC,k-1}}$$

Applying the same procedure to all $T_{IVC,k-1}$ terms and substituting them back into Eq. (47), results in a linear equation relating model input, output and state variables (in red) in terms of the operating point ($\bar{\alpha}_k$, $\overline{T_{IVC,k}}$, $\overline{\alpha_{k-1}}$, $\overline{T_{IVC,k-1}}$). The final linear equation is shown in Eq. (48).

$$(c_1+c_2\bar{\alpha}_k)\,\widetilde{T_{IVC,k}}=c_1\widetilde{T_{in,k}}$$

$$+\tilde{\alpha}_k\begin{pmatrix}-c_2\overline{T_{IVC,k}}+\beta_1\beta_{19}\overline{T_{IVC,k-1}}^{1-n}-\beta_2\beta_{19}\overline{T_{IVC,k-1}}^{1-n}\overline{\alpha_{k-1}}-\beta_3\beta_{19}\overline{T_{IVC,k-1}}^{1-n}\overline{\alpha_{k-1}}^{2}\\+\beta_4\beta_{19}\overline{T_{IVC,k-1}}^{2-n}+\xi_1\beta_{19}\overline{T_{IVC,k-1}}^{2-n}\overline{\alpha_{k-1}}+\xi_2\beta_{19}\overline{T_{IVC,k-1}}^{2-n}\overline{\alpha_{k-1}}^{2}-\beta_9\beta_{19}\overline{T_{IVC,k-1}}^{2-n}\overline{\alpha_{k-1}}^{3}\\+\beta_{10}\beta_{19}\overline{T_{IVC,k-1}}^{3-n}+\xi_3\beta_{19}\overline{T_{IVC,k-1}}^{3-n}\overline{\alpha_{k-1}}+\xi_4\beta_{19}\overline{T_{IVC,k-1}}^{3-n}\overline{\alpha_{k-1}}^{2}+\xi_5\beta_{19}\overline{T_{IVC,k-1}}^{3-n}\overline{\alpha_{k-1}}^{3}\\-\beta_{18}\beta_{19}\overline{T_{IVC,k-1}}^{3-n}\overline{\alpha_{k-1}}^{4}\end{pmatrix}$$

$$+\widetilde{\alpha_{k-1}}\begin{pmatrix}-\beta_2\beta_{19}\bar{\alpha}_k\overline{T_{IVC,k-1}}^{1-n}-2\beta_3\beta_{19}\bar{\alpha}_k\overline{T_{IVC,k-1}}^{1-n}\overline{\alpha_{k-1}}+\beta_{19}\xi_1\bar{\alpha}_k\overline{T_{IVC,k-1}}^{2-n}\\+2\xi_2\beta_{19}\bar{\alpha}_k\overline{T_{IVC,k-1}}^{2-n}\overline{\alpha_{k-1}}-3\beta_9\beta_{19}\bar{\alpha}_k\overline{T_{IVC,k-1}}^{2-n}\overline{\alpha_{k-1}}^{2}+\xi_3\beta_{19}\bar{\alpha}_k\overline{T_{IVC,k-1}}^{3-n}\\+2\xi_4\beta_{19}\bar{\alpha}_k\overline{T_{IVC,k-1}}^{3-n}\overline{\alpha_{k-1}}+3\xi_5\beta_{19}\bar{\alpha}_k\overline{T_{IVC,k-1}}^{3-n}\overline{\alpha_{k-1}}^{2}-4\beta_{18}\beta_{19}\bar{\alpha}_k\overline{T_{IVC,k-1}}^{3-n}\overline{\alpha_{k-1}}^{3}\end{pmatrix}$$

$$+\widetilde{T_{IVC,k-1}}\begin{pmatrix}\beta_1\beta_{20}\bar{\alpha}_k-\beta_2\beta_{20}\bar{\alpha}_k\overline{\alpha_{k-1}}-\beta_3\beta_{20}\bar{\alpha}_k\overline{\alpha_{k-1}}^{2}+\beta_4\beta_{21}\bar{\alpha}_k+\xi_1\beta_{21}\bar{\alpha}_k\overline{\alpha_{k-1}}+\xi_2\beta_{21}\bar{\alpha}_k\overline{\alpha_{k-1}}^{2}\\-\beta_9\beta_{21}\bar{\alpha}_k\overline{\alpha_{k-1}}^{3}+\beta_{10}\beta_{22}\bar{\alpha}_k+\xi_3\beta_{22}\bar{\alpha}_k\overline{\alpha_{k-1}}+\xi_4\beta_{22}\bar{\alpha}_k\overline{\alpha_{k-1}}^{2}+\xi_5\beta_{22}\bar{\alpha}_k\overline{\alpha_{k-1}}^{3}\\-\beta_{18}\beta_{22}\bar{\alpha}_k\overline{\alpha_{k-1}}^{4}\end{pmatrix}\quad(48)$$

The term $\widetilde{T_{in,k}}$ in Eq. (48) is neither an input, output nor state variable and hence has to be removed to make Eq. (48) a valid input-output linear relationship. The inlet temperature $\widetilde{T_{in,k}}$ is a variable that can be considered as another control input. Therefore,

the model presented in Eq. (48) is currently a multi-input single-output (MISO) system. To make the control system less complex, it is preferable to convert the MISO system into a single-input single-output system (SISO). To eliminate the second input, $T_{in,k}$, a linear relationship between α_k and $T_{in,k}$ is assumed, Eq. (49).

$$T_{in,k} = 300 + 175\alpha_k \tag{49}$$

This relationship was developed by looking at the ranges of both α_k (0 – 0.4) and $T_{in,k}$ (300 – 370) and interpolating a linear equation between the lower and upper ranges of both variables. By implementing this assumption, the system is now SISO and $T_{in,k}$ is changing within a reasonable range when varying α_k.

Substituting Eq. (49) into Eq. (48) results in the following final linear equation that is now in terms of model state variables only:

$$(c_1 + c_2\bar{\alpha}_k)\,\widetilde{T_{IVC,k}} = 300\,c_1$$

$$+\,\tilde{\alpha}_k \begin{pmatrix} 175\,c_1 - c_2\overline{T_{IVC,k}} + \beta_1\beta_{19}\overline{T_{IVC,k-1}}^{1-n} - \beta_2\beta_{19}\overline{T_{IVC,k-1}}^{1-n}\overline{\alpha_{k-1}} - \beta_3\beta_{19}\overline{T_{IVC,k-1}}^{1-n}\overline{\alpha_{k-1}}^2 \\ + \beta_4\beta_{19}\overline{T_{IVC,k-1}}^{2-n} + \xi_1\beta_{19}\overline{T_{IVC,k-1}}^{2-n}\overline{\alpha_{k-1}} + \xi_2\beta_{19}\overline{T_{IVC,k-1}}^{2-n}\overline{\alpha_{k-1}}^2 - \beta_9\beta_{19}\overline{T_{IVC,k-1}}^{2-n}\overline{\alpha_{k-1}}^3 \\ + \beta_{10}\beta_{19}\overline{T_{IVC,k-1}}^{3-n} + \xi_3\beta_{19}\overline{T_{IVC,k-1}}^{3-n}\overline{\alpha_{k-1}} + \xi_4\beta_{19}\overline{T_{IVC,k-1}}^{3-n}\overline{\alpha_{k-1}}^2 + \xi_5\beta_{19}\overline{T_{IVC,k-1}}^{3-n}\overline{\alpha_{k-1}}^3 \\ - \beta_{18}\beta_{19}\overline{T_{IVC,k-1}}^{3-n}\overline{\alpha_{k-1}}^4 \end{pmatrix}$$

$$+\,\widetilde{\alpha_{k-1}} \begin{pmatrix} -\beta_2\beta_{19}\bar{\alpha}_k\overline{T_{IVC,k-1}}^{1-n} - 2\beta_3\beta_{19}\bar{\alpha}_k\overline{T_{IVC,k-1}}^{1-n}\overline{\alpha_{k-1}} + \beta_{19}\xi_1\bar{\alpha}_k\overline{T_{IVC,k-1}}^{2-n} \\ +2\xi_2\beta_{19}\bar{\alpha}_k\overline{T_{IVC,k-1}}^{2-n}\overline{\alpha_{k-1}} - 3\beta_9\beta_{19}\bar{\alpha}_k\overline{T_{IVC,k-1}}^{2-n}\overline{\alpha_{k-1}}^2 + \xi_3\beta_{19}\bar{\alpha}_k\overline{T_{IVC,k-1}}^{3-n} \\ +2\xi_4\beta_{19}\bar{\alpha}_k\overline{T_{IVC,k-1}}^{3-n}\overline{\alpha_{k-1}} + 3\xi_5\beta_{19}\bar{\alpha}_k\overline{T_{IVC,k-1}}^{3-n}\overline{\alpha_{k-1}}^2 - 4\beta_{18}\beta_{19}\bar{\alpha}_k\overline{T_{IVC,k-1}}^{3-n}\overline{\alpha_{k-1}}^3 \end{pmatrix}$$

$$+\,\widetilde{T_{IVC,k-1}} \begin{pmatrix} \beta_1\beta_{20}\bar{\alpha}_k - \beta_2\beta_{20}\bar{\alpha}_k\overline{\alpha_{k-1}} - \beta_3\beta_{20}\bar{\alpha}_k\overline{\alpha_{k-1}}^2 + \beta_4\beta_{21}\bar{\alpha}_k + \xi_1\beta_{21}\bar{\alpha}_k\overline{\alpha_{k-1}} + \xi_2\beta_{21}\bar{\alpha}_k\overline{\alpha_{k-1}}^2 \\ -\beta_9\beta_{21}\bar{\alpha}_k\overline{\alpha_{k-1}}^3 + \beta_{10}\beta_{22}\bar{\alpha}_k + \xi_3\beta_{22}\bar{\alpha}_k\overline{\alpha_{k-1}} + \xi_4\beta_{22}\bar{\alpha}_k\overline{\alpha_{k-1}}^2 + \xi_5\beta_{22}\bar{\alpha}_k\overline{\alpha_{k-1}}^3 \\ -\beta_{18}\beta_{22}\bar{\alpha}_k\overline{\alpha_{k-1}}^4 \end{pmatrix} \tag{50}$$

Eq. (50) can be expressed in a simplified format:

$$V\,T_{IVC,k} = W\alpha_k + X\alpha_{k-1} + YT_{IVC,k-1} + Z \tag{51}$$

where V, W, X and Y are functions in terms of $\bar{\alpha}_k$, $\overline{T_{IVC,k}}$, $\overline{\alpha_{k-1}}$, and $\overline{T_{IVC,k-1}}$.

Ignoring the constant Z for now, the linear model of Eq. (51) can be used to develop the state-space representation of the HCCI control model. The final state-space form of the model is:

$$\begin{bmatrix} \alpha_k \\ T_{IVC,k} \end{bmatrix} = \begin{bmatrix} 0 & 0 \\ X/V & Y/V \end{bmatrix} \begin{bmatrix} \alpha_{k-1} \\ T_{IVC,k-1} \end{bmatrix} + \begin{bmatrix} 1 \\ W/V \end{bmatrix} \alpha_k$$

$$y = \begin{bmatrix} 0 & 1 \end{bmatrix} \begin{bmatrix} \alpha_{k-1} \\ T_{IVC,k-1} \end{bmatrix} \tag{52}$$

To verify the accuracy of the developed model, it has to be validated against the nonlinear model of Eq. (41). Details and results of the validation are explained in the next subsection.

3.4 Validation of the Developed Linear Model

Before validating the linear model, an operating point must be chosen to linearize the nonlinear model about. Several operating points are chosen (Table 3.1) and are used to determine the values of the variables V, W, X and Y. The final values of V, W, X and Y will be calculated based on the operating point which provides results that match the data produced by the nonlinear model.

Each operating point is applied to the linear model (Eq. (50) which is simulated in MATLAB to determine V, W, X and Y. At each value of V, W, X, and Y, a step input, α_k, is applied to both linear and nonlinear models and the results were compared.

Table 3.1 Operating points chosen for validation

Operating Point	P_{IVC} (kPa)	α_k (%)	α_{k-1} (%)	$T_{IVC,k-1}$ (K)	$T_{IVC,k}$ (K)	θ_{SOC} (CA aTDC)
1	122	0	0	440	440	-9.8
2	101	0.1	0	370	370	-3
3	101	0.2	0	450	450	-8.2
4	101	0.3	0	390	390	-4.2
5	101	0.4	0	410	410	-5.5

Linearizing about operating point 4 was found to yield results closely matching to those obtained from the non-linear model. Figure 3.2 compares the output of both linear and nonlinear models at a step input of $\alpha_k = 0.2$ and $\theta_{SOC} = -4$ CA aTDC.

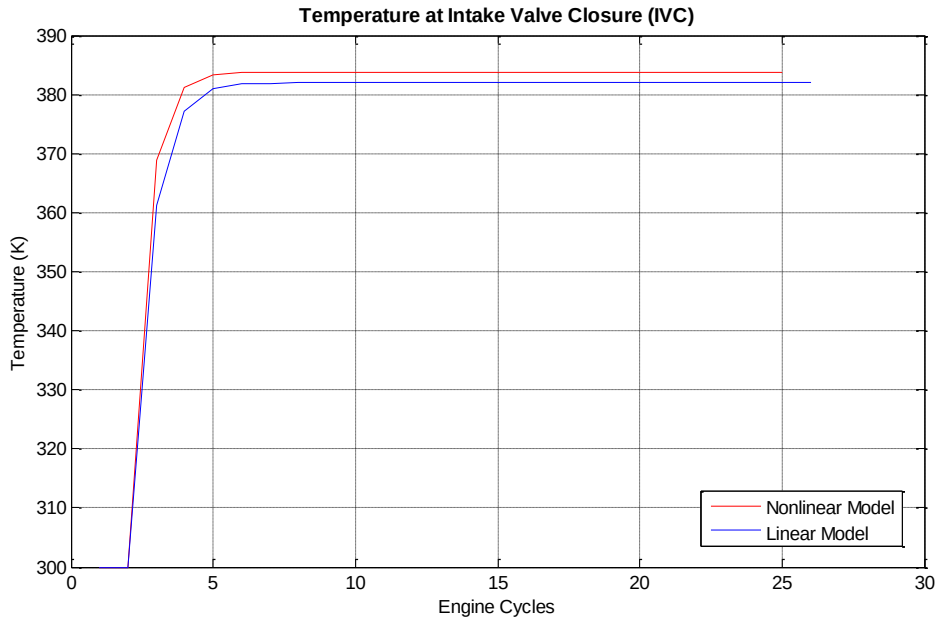

Figure 3.2 Output generated using nonlinear and linear models at constant input

As shown in Figure 3.2, the nonlinear model reaches a value of 383.78 K while the linear model reaches a value of 381.99 K. The error is about 0.5% which shows that

the model linearized about operating point 4 is a successful representation of the nonlinear model. Hence, this model can be used to develop the required controller which is the topic of discussion of the next section.

3.5 Conclusions

After confirming that the nonlinear model developed in Section 2 can predict ignition timing accurately, a closed-loop control model was designed to control ignition timing. The input, output and state variables were determined where the output of the model was chosen to be temperature at IVC rather than ignition timing for practical purposes.

An input-output relationship was developed based on the thermodynamical equations in Section 2. As expected, the relationship was highly nonlinear since the equations used were nonlinear. In order to apply linear control strategies, the obtained input-output relationship was linearized. Binomial expansion and defining new constants were methods that were used to simplify the relationship and facilitate the linearization process.

The perturbation method was used to linearize the function. This method primarily depended on substituting the model variables with their linear expansions and then neglecting fluctuations of an order more than one due to their infinitesimal value. Finally, a linear model was developed in terms of the chosen system input, output and state variables and the final state-space form of the model was obtained. The linear model is now ready to be used in the implementation of the controller as will be shown in Section 4.

4. IMPLEMENTATION OF A LINEAR QUADRATIC REGULATOR CONTROLLER

In Section 3, a linear model for the HCCI engine was developed in order to be implemented on a linear controller. In this section, a Linear Quadratic Regulator (LQR) is designed based on the obtained linear model to control the ignition timing of HCCI engine. Due to the nature of the developed linear model, a feedforward control path is needed as well. This section explains the design process of both the LQR and feedforward controllers. The robustness of the control model when implemented on the linear model is also tested, before applying it to the nonlinear model. In addition, the ability for the control model to reject disturbance and parameter variation is also discussed.

4.1 LQR Basics

Optimal control is a powerful control strategy which aims to optimize an objective function while maintaining the closed-loop system stability. The objective function is mainly an important aspect of a system whose successful operation largely depends on. It generally relates the performance of the system to a cost or energy consumption criterion for the full system's operating envelop, i.e., $J_1 = \int_0^T |u(\tau)| d\tau$, where u is the control authority. Since there is no analytical solution for this functional, an alternate criterion $J_2 = \int_0^T u(\tau)^T u(\tau)\, d\tau$ is utilized in practice instead. The optimal control theory, hence, deals with designing a control system which optimizes or namely minimizes the represented cost function while stabilizing the system closed-loop

dynamics. The most widely used optimal control approach which additionally takes into account the system states in the cost function definition is perhaps the LQR. LQR regulates the system dynamics with the optimal control obtained based on the linear quadratic terms of the system's inputs and states.

When using the pole placement method, a linear control law is developed such that:

$$u(t) = -Kx(t) \tag{53}$$

where u(t) is the input, K is the gain vector and x(t) is the states vector of the system. When designing a LQR controller, rather than finding a gain matrix, K, that would achieve the specified closed-loop locations, a gain matrix is developed to minimize the cost function, V [63]:

$$V = \int_t^T [x^T(\tau)Q(\tau)x(\tau) + u^T(\tau)R(\tau)u(\tau)]\, d\tau \tag{54}$$

where Q and R are symmetric matrices, t is the present time and T is the terminal time. For stable steady state solution, when $T = \infty$,

$$V_\infty = \int_t^\infty [x^T Q\, x + u^T R\, u\,]\, d\tau \tag{55}$$

will converge to the following criterion with a constant performance matrix, P.

$$\therefore V_\infty = x^T P\, x \tag{56}$$

where P satisfies the following positive algebraic quadratic equation, or namely, the algebraic Riccati equation:

$$0 = PA + A^T P - PBR^{-1}B^T P + Q \tag{57}$$

The optimum gain matrix is computed by:

$$K = R^{-1}B^T P \tag{58}$$

Hence [63],

(a) If the system is asymptotically stable (i.e. the eigenvalues of matrix A of the state-space system, or the open-loop poles of the system, are negative) or

(b) the system is controllable and observable,

then the algebraic Riccati equation has a unique, positive definite solution P which minimizes V_∞ when the control law is $u = - R^{-1}B^T P x$.

4.2 Controller Development

A LQR controller can be applied to the final state-space model developed in Section 3 to control combustion timing through controlling temperature at intake valve closure (T_{IVC}). This process can be seen as a regulation problem where the aim is to regulate T_{IVC} to maintain combustion timing. In this case, the output is changed from being T_{IVC} to being the error between the actual T_{IVC} and the desired T_{IVC}. As a result, the LQR controller is developed to minimize the error.

In Section 3.3, the final linear model was defined as:

$$V\, T_{IVC,k} = W\alpha_k + X\alpha_{k-1} + YT_{IVC,k-1} + Z \tag{51}$$

where α_k is the input, $T_{IVC,k-1}$ is the output, and α_{k-1} and $T_{IVC,k-1}$ are the model states. In order to regulate the output, a new variable is defined as the error between the actual output, y, and the desired output, y*:

$$e = y^* - y \tag{59}$$

where

$$y = T_{IVC,k-1}$$

$$y^* = T_{IVC,k-1}{}^*$$

Differentiating the error yields the following:

$$\dot{e} = \dot{y}^* - \dot{y} = T_{IVC,k}{}^* - T_{IVC,k} \tag{60}$$

Substituting Eq. (51) into Eq. (60) results in:

$$\dot{e} = \dot{y}^* - \dot{y} = T_{IVC,k}{}^* - \frac{W}{V}\alpha_k - \frac{X}{V}\alpha_{k-1} - \frac{Y}{V}T_{IVC,k-1} - \frac{Z}{V} \tag{61}$$

Using Eq. (59) to substitute the value of $T_{IVC,k-1}$ in Eq. (61) and simplifying the final equation results in the following:

$$\dot{e} = \dot{y}^* - \dot{y} = T_{IVC,k}{}^* - W'\alpha_k - X'\alpha_{k-1} - Y'(y^* - e) - Z' \tag{62}$$

where:

$$W' = \frac{W}{V}, X' = \frac{X}{V}, Y' = \frac{Y}{V} \text{ and } Z' = \frac{Z}{V}$$

Re-writing Eq. (62) in discrete form yields:

$$e_k = Y'e_{k-1} - W'\alpha_k - X'\alpha_{k-1} - Y'y^* - Z' + T_{IVC,k}{}^* \tag{63}$$

The state-space form of the system can be re-written to define the output to be the error instead of $T_{IVC,k-1}$. Letting $- Y'y^* - Z' + T_{IVC,k}{}^* = T^*$, the final state-space form of the system is:

$$\begin{bmatrix}\alpha_k \\ e_k\end{bmatrix} = \begin{bmatrix}0 & 0 \\ -X' & Y'\end{bmatrix}\begin{bmatrix}\alpha_{k-1} \\ e_{k-1}\end{bmatrix} + \begin{bmatrix}1 \\ -W'\end{bmatrix}\alpha_k + \begin{bmatrix}0 \\ 1\end{bmatrix}T^* \tag{64}$$

$$y = \begin{bmatrix}0 & 1\end{bmatrix}\begin{bmatrix}\alpha_{k-1} \\ e_{k-1}\end{bmatrix} \tag{65}$$

Eqs. (64) and (65) can be written in general state-space form to the following:

$$x_k = Ax_{k-1} + Bu_k + MT^* \tag{66}$$

$$y_{k-1} = Cx_{k-1} \tag{67}$$

Due to the addition of the extra variable T* to the system, the state-space form is not of the standard form:

$$\dot{x} = Ax + Bu$$

$$y = Cx + Du$$

Therefore such a "disturbance-like" behavior will be compensated through a feedforward loop and will be further included within the control law. As discussed in Section 4.1, the customary LQR control law is defined as:

$$u(t) = -Kx(t) \tag{53}$$

Eq. (53) can be re-written in discrete from as:

$$u_k = -Kx_{k-1} \tag{68}$$

Adding the feedforward component, the new control law becomes:

$$u_k = -Kx_{k-1} + u_F \tag{69}$$

where u_F represents the input required for the feedfoward.

Substituting Eq. (69) into Eq. (66) includes the new control law within the system state-space and results in the following:

$$x_k = (A - BK)\, x_{k-1} + Bu_F + MT^* \tag{70}$$

The next step would be to figure out how to calculate u_F. The control input $u_F = -B^{-1}MT^*$ is feedforwarded to the system to cancel out the effect of the third term in the right-hand side of Eq. (70). However, matrix B requires pseudo-inverse in order to be used in the feedforward control.

Since this problem is seen as a regulation type problem, the system is assumed to be in steady-state. As a result, the derivatives of the system tend to zero which means x_k in Eq. (66) will be equated to 0 and the following expression for x_{k-1} is deduced:

$$x_{k-1} = -[\bar{A}]^{-1}\left(MT^{*} + Bu_F\right) \tag{71}$$

where:

$$\bar{A} = A - BK$$

In addition, as explained before, the goal of the LQR is to minimize the error. Therefore, the output, y_{k-1} (Eq. (67)) tends to 0 which means x_{k-1} in Eq. (71) becomes 0. As a result, u_F is calculated using the following formula:

$$u_F = -(C\,\bar{A}^{-1}B)^{-1}\left(C\bar{A}^{-1}MT^{*}\right) \tag{72}$$

Now most of the unknown variables (A, B, C, M, T* and u_F) of the system in state-space form can be calculated. The only variable missing is the gain vector K, which contains the LQR gains needed to complete the control law. These gains are found using MATLAB's LQR function. The inputs to the LQR function are the original system matrices: A, B and C in Eqs. (64) and (65) without including the feedforward component, i.e. MT^{*}. A, B and C matrices need to be calculated through determining the values of V, W, X, Y and Z using Eq. (50) which will depend on the chosen operating point. As demonstrated in Section 3, the linear model follows the nonlinear model around operating point 4 (Table 3.1). Subsequently, the LQR gains can be calculated using MATLAB. In the next subsection, the new control law is implemented on the

system and the final model is evaluated based on how well the output can track a desired value.

4.3 Implementation and Validation of LQR Controller

By linearizing the nonlinear model about operating point 4 in Table 3.1, the values of V, W, X, Y and Z of Eq. (51) can be determined as in Table 4.1. Substituting the values in Table 4.1 into Eq. (64) provides the values for matrices A and B of the state-space model. Vector C can be obtained from Eq. (65).

Table 4.1 Values of linear model parameters

Variable	Value (Unitless)
V	0.3901
W	122.6513
X	4.1552
Y	0.0888
Z	300

To calculate the LQR gains it is necessary to assume Q and R matrices that are positive definite. Q and R matrices have been assumed as:

$$Q = \begin{bmatrix} 1 & 0 \\ 0 & 1 \end{bmatrix}, \quad R = [1] \tag{73}$$

Using the values of these matrices, the gain matrix can be obtained using the algebraic Riccati equation in Eq. (58). To complete determining the control law, u_F is yet to be calculated using Eq. (72). The LQR controller is now ready to be implemented on both the linear and nonlinear model.

To evaluate the performance of the controller, a desired output, $T^*_{IVC,k-1}$, is used as an input and the model is verified based on how well it tracks the desired output. Figure 4.1 shows the block diagram of the linear system after implementing the LQR and feedforward controller.

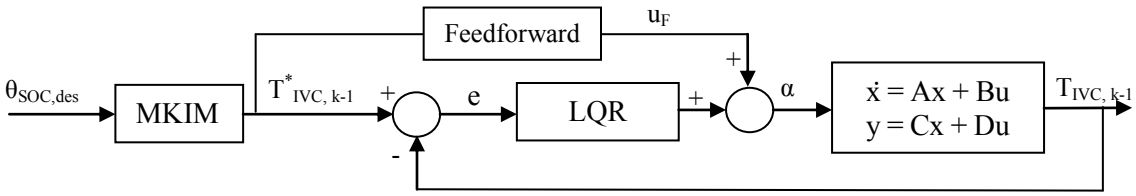

Figure 4.1 Block diagram of LQR and feedforward controller implemented on the linear model

Figures 4.2 and 4.3 show the responses of the linear model while tracking desired outputs of 350K and 400K.

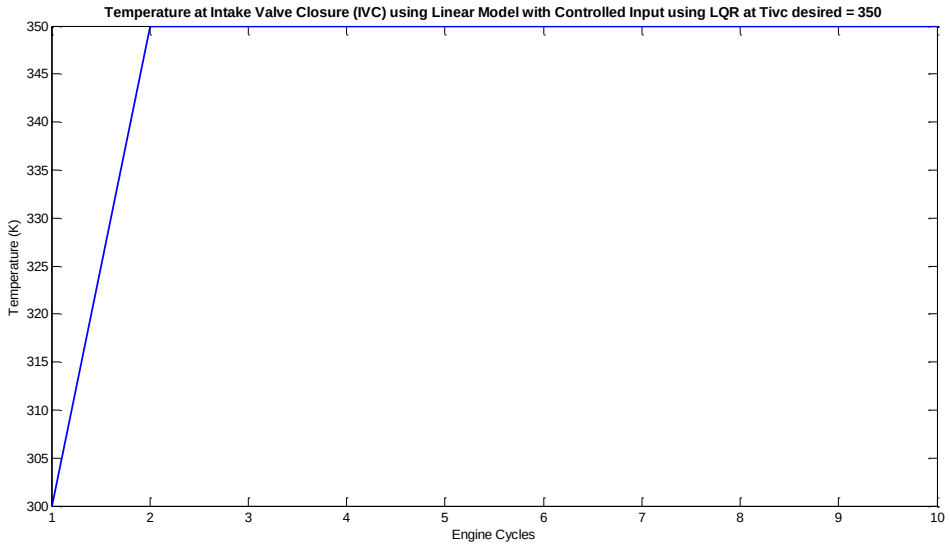

Figure 4.2 Output response of the linear model controlled with the LQR, tracking a desired output of 350K

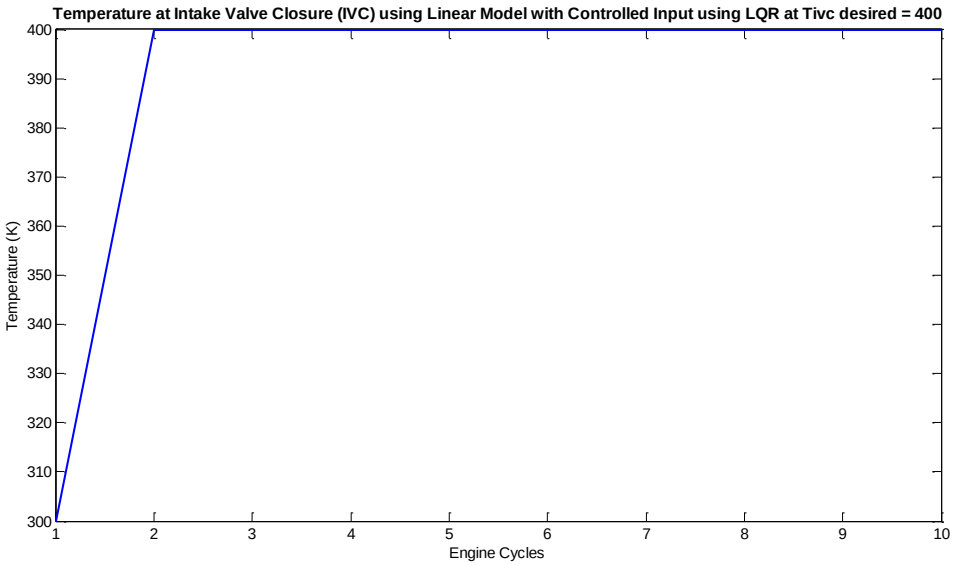

Figure 4.3 Output response of the linear model controlled with the LQR, tracking a desired output of 400K

As can be seen in Figures 4.2 and 4.3, the linear model is able to track the exact desired output.

4.4 Robustness of LQR Controller

The LQR controllers perform robustly with respect to process uncertainty Δ shown in Figure 4.4 where $|\Delta| \leq$ L. The term L can be chosen smaller than 0.5 based on the Kalman's inequality which guarantees $\left|\frac{G(s)}{1+G(s)}\right| \leq 2$ [64].

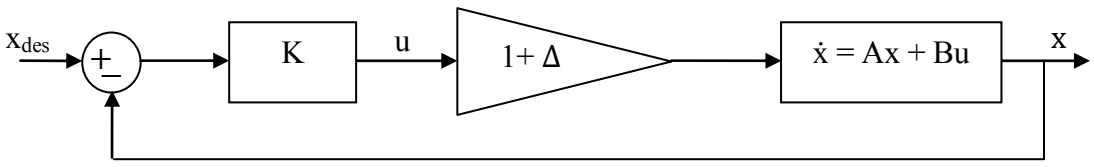

Figure 4.4 Block diagram of LQR controller with added disturbance implemented on the linear model

Performance of the control system is shown in Figures 4.5 and 4.6 for the linear system against a disturbance $|\Delta| = 0.5$ while tracking a desired output of 400K. The control input is added at cycle 2 that causes the sudden increase in Figure 4.5. The control input then slowly decreases until it reaches a steady-state value. Figure 4.6 shows that the output with no disturbance added to the linear system is overlapping over the output when a disturbance of $\Delta = 0.5$ (+50% disturbance on the control input, EGR ratio) is added. This indicates that the LQR controller can reject the disturbance and perform satisfactorily.

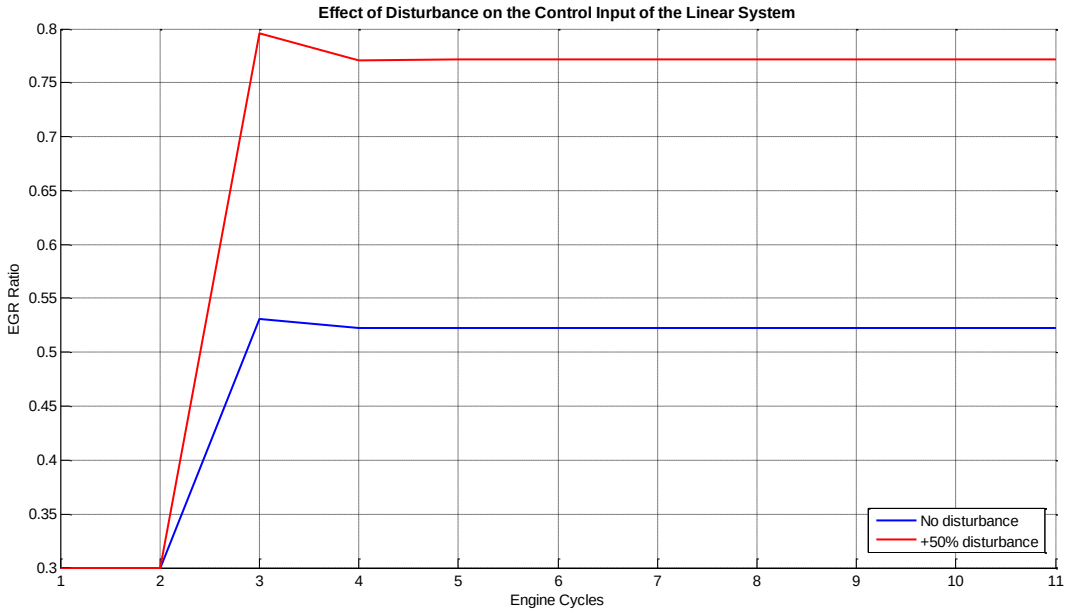

Figure 4.5 Effect of disturbance on the control input of the linear system

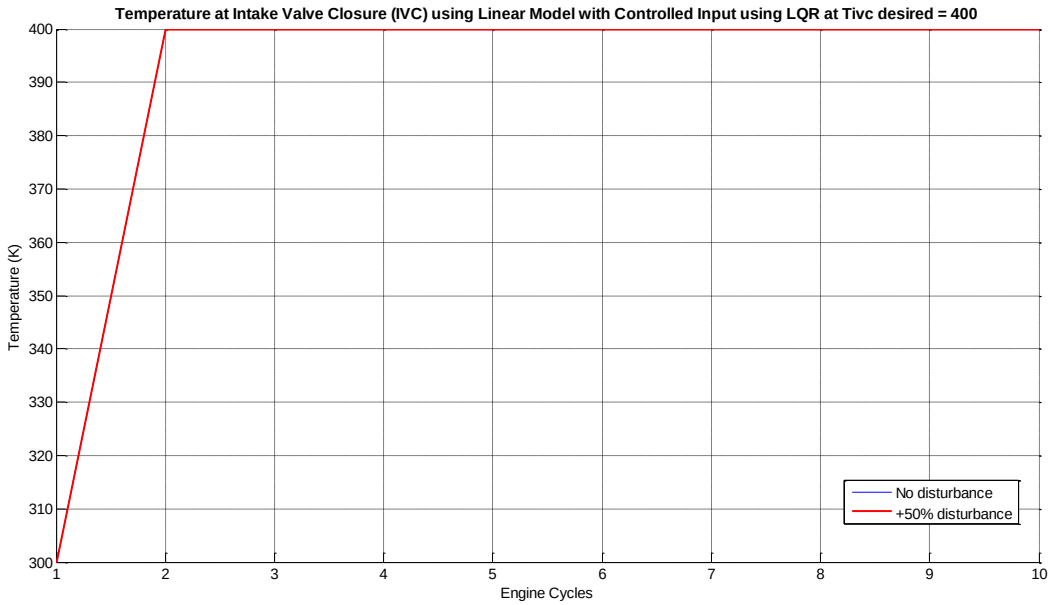

Figure 4.6 Effect of disturbance on the output of the linear system

After the successful implementation of LQR controller on the linear model, it can now be applied to the nonlinear model.

Figure 4.7 shows the block diagram of the nonlinear model with LQR and feedforward control implementation.

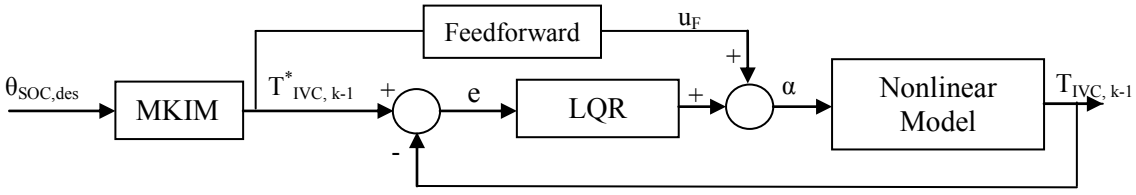

Figure 4.7 Block diagram of LQR and feedforward controller implemented on the nonlinear model

Figures 4.8 and 4.9 show the responses of the non-linear model while tracking specified desired outputs of 370K and 400K. As can be seen in Figures 4.8 and 4.9, the nonlinear model was able to track the desired temperature with an error less than 0.5%. In Figure 4.8, the error is about 0.48%, while the error in Figure 4.9 is about 0.4%. Hence, the developed LQR controller has succeeded to control the combustion timing of an HCCI engine model through controlling the temperature at IVC, T_{IVC}.

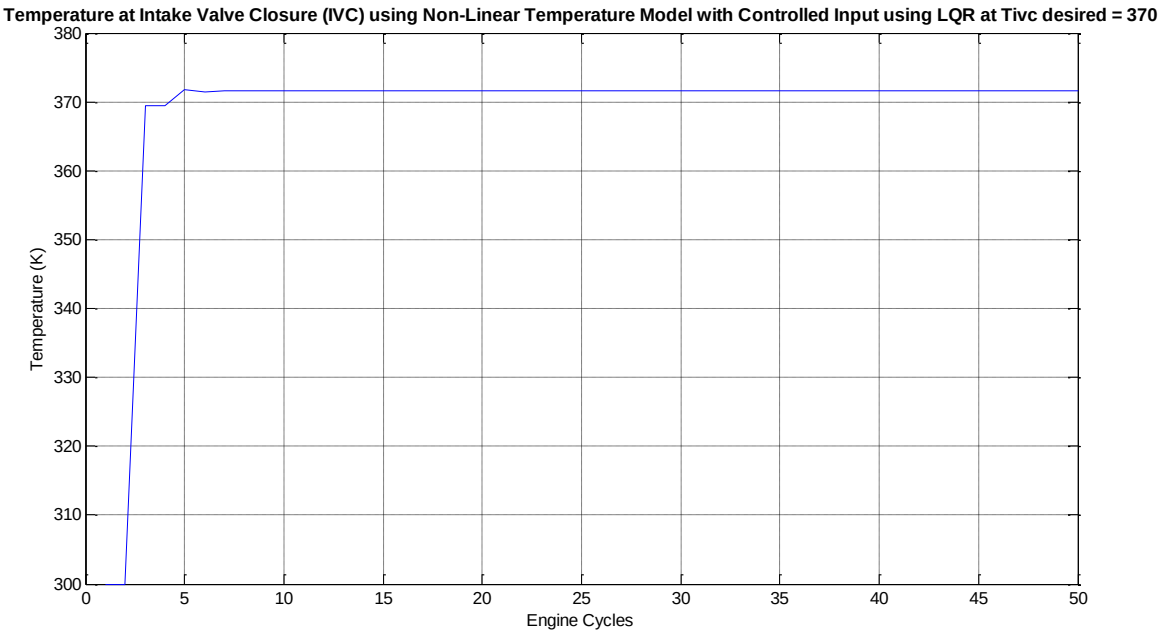

Figure 4.8 Output response of the nonlinear model controlled with the LQR, tracking a desired output of 370K

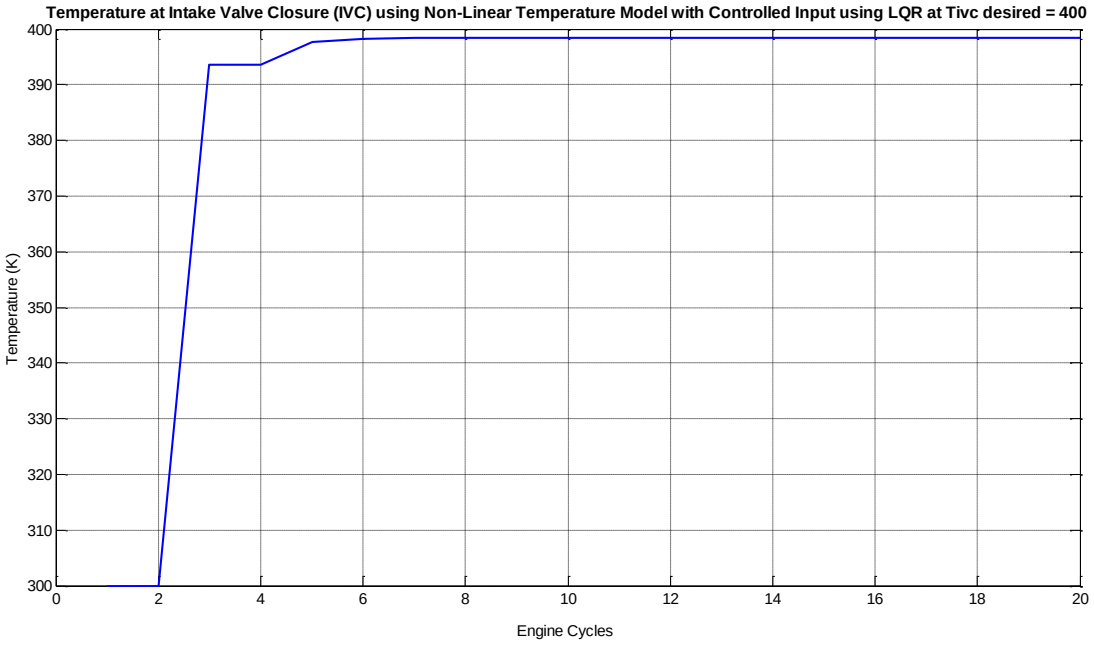

Figure 4.9 Output response of the nonlinear model controlled with the LQR, tracking a desired output of 400K

4.5 LQR Operating Range

Since the nonlinear model was linearized about an operating point, the obtained linear model will perform at its best when the desired output is around the operating point. Therefore, it is important to understand the operating range in which the controller can work at its best.

While testing the performance of the controller when regulating the nonlinear model, the operating range is determined by maintaining the error within 0.5%. It is found that the nonlinear model can track the desired output with an error less than 0.5% when the desired output is within the range 370K–415K. This operating range is valid when the nonlinear model is linearized about operating point 4 (T_{IVC} = 390K) in Table 3.1. If the nonlinear model is needed to track an output more than 415K or less than

370K, the error is more than 0.5% as shown in Figures 4.10 and 4.11. In Figure 4.10, the output is 352.78K which results in an error of 0.8% since the desired T_{IVC} is 350K. In Figure 4.11, the error was 2% for a desired T_{IVC} of 450K.

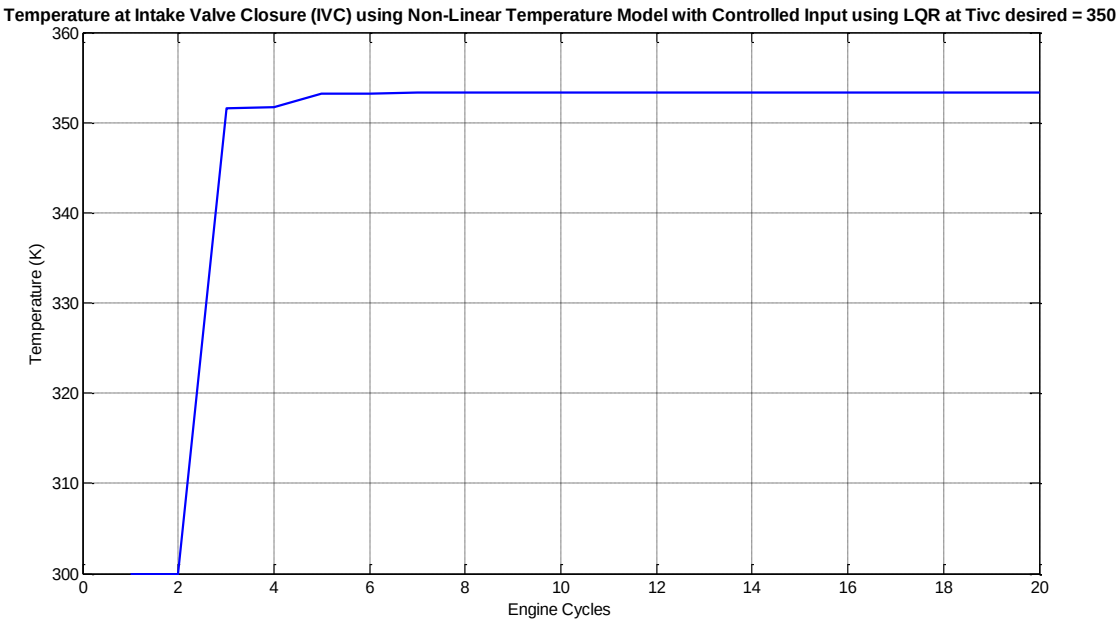

Figure 4.10 Output response of the nonlinear model controlled with the LQR, tracking a desired output of 350K

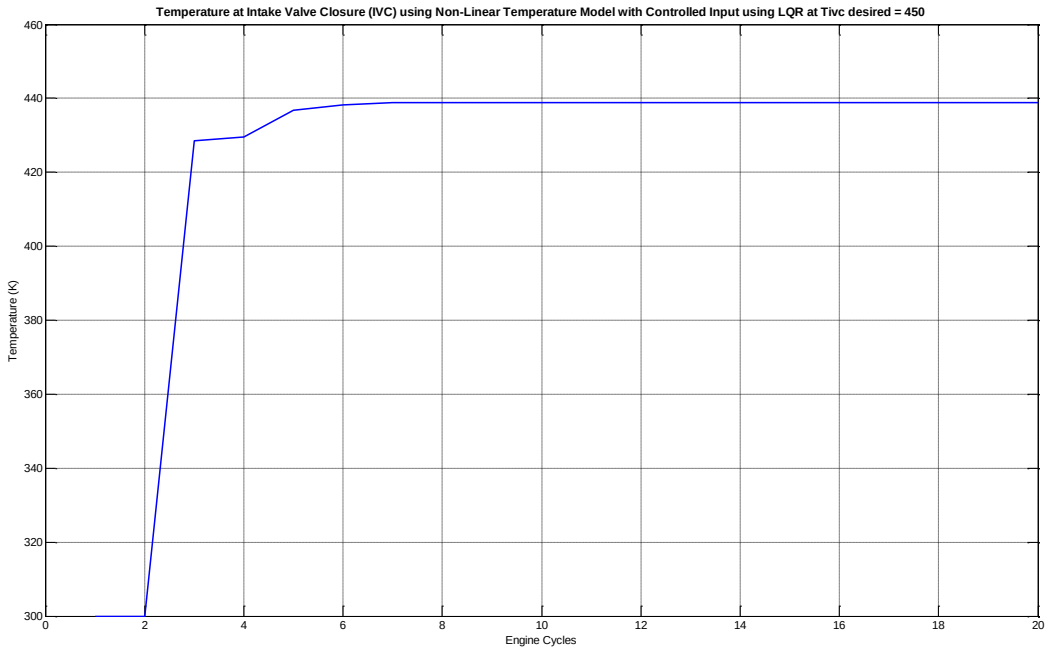

Figure 4.11 Output response of the nonlinear model controlled with the LQR, tracking a desired output of 450K

In an attempt to increase the operating range of the LQR controller, an integrator was added to cancel the steady state errors since the standard LQR only provides proportional gains. To compare the performance of the controller with and without the integral action, the desired T_{IVC} was chosen to be 350K and 450K and the output was compared to Figures 4.10 and 4.11 respectively.

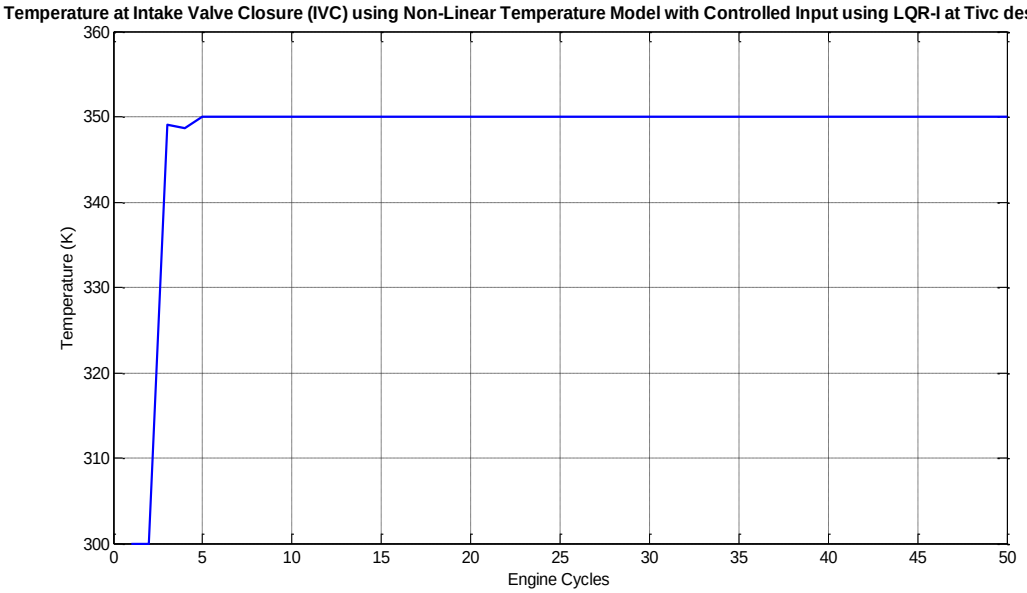

Figure 4.12 Output response of the nonlinear model controlled with the LQR and integral action, tracking a desired output of 350K

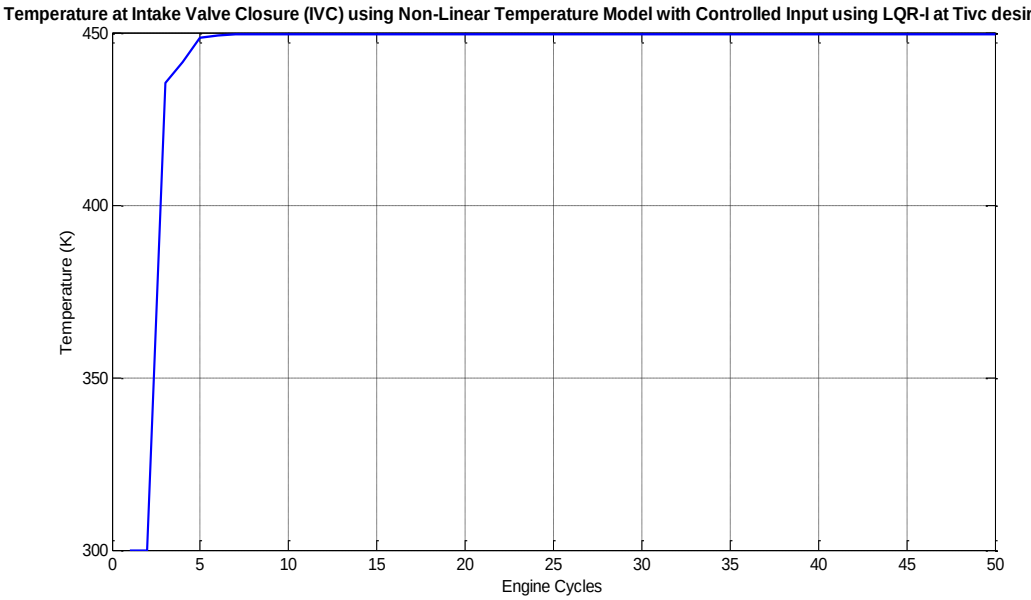

Figure 4.13 Output response of the nonlinear model controlled with the LQR and integral action, tracking a desired output of 450K

Comparing the output in Figures 4.10 and 4.12, it is noticeable that the error has decreased. In Figure 4.12, the output temperature is about 350K which resulted in an approximate error of 0.01% instead of 0.8% which was observed in Figure 4.10. Similarly, when the desired output was 450K, the error decreased from 2% to approximately 0.1% after adding the integrator. Hence, adding the integral resulted in the successful removal of the steady-state error in the system, therefore increasing the operating range to 330K – 460K. Figure 4.14 shows the final block diagram of the control model with the added integrator.

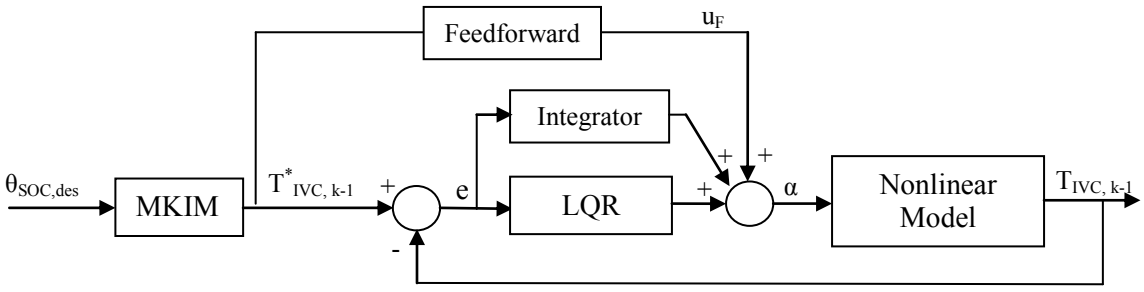

Figure 4.14 Block diagram of LQR and feedforward controller with the added integrator implemented on the nonlinear model

4.6 Disturbance and Parameter Variation

It is important to test the closed-loop performance of the designed controller to understand how well it performs under disturbance and change in parameters. The disturbances can be categorized to be one of the following:

a) Disturbance caused by actuator

b) Parameter variation

Each of the above is applied to the control model to investigate how well the controller can reject these disturbances.

4.6.1 Actuator Disturbance

This type of disturbance is assumed to occur when one of the actuators in the system is not working properly. In the current engine setup, the most important actuator is the EGR valve which is responsible for re-inducting exhaust gases back into the cylinder. It also represents the control input of the closed-loop system.

To test how well the controller can handle disturbances in the control input, a gain of $\pm 5\%$ has been added to the control input, as shown in the block diagram below:

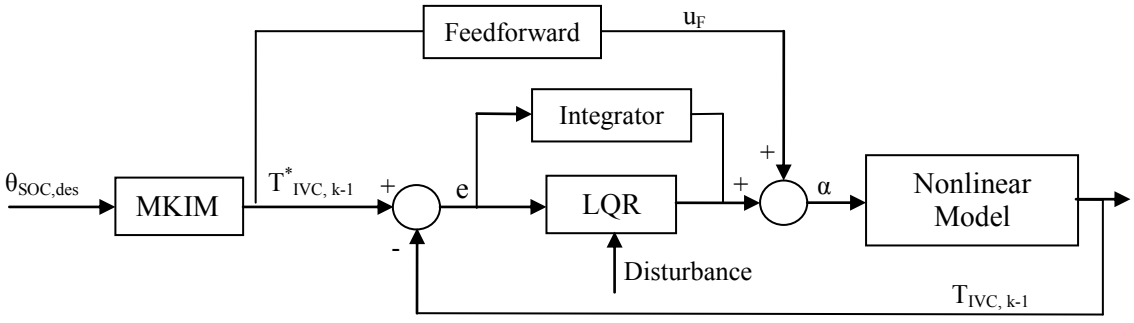

Figure 4.15 Block diagram showing the added actuator disturbance to the final system

Figures 4.16 and 4.17 show the effect of the added disturbance on both the input and output of the system respectively. The effect of adding the disturbance can be seen on both the input and output where the plot deviates from the original system when no disturbance is added. Specifically, the disturbance caused the output to deviate with an error of -0.6% and 0.9% when a -5% and +5% disturbance was added, respectively. In

addition to the relatively small deviation, it is also visible that the error decreases as the simulation continues to run. Therefore, it is safe to assume that eventually the disturbed output will converge to the desired temperature output. Hence, the controller is able to slowly reject actuator disturbances.

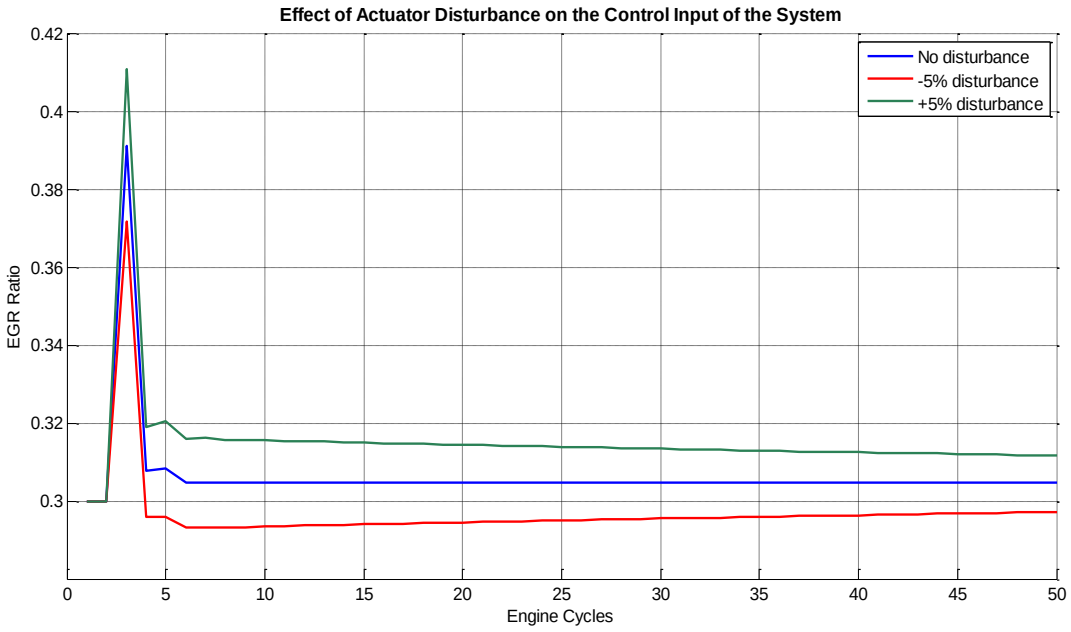

Figure 4.16 Effect of actuator disturbance on the control input of the system

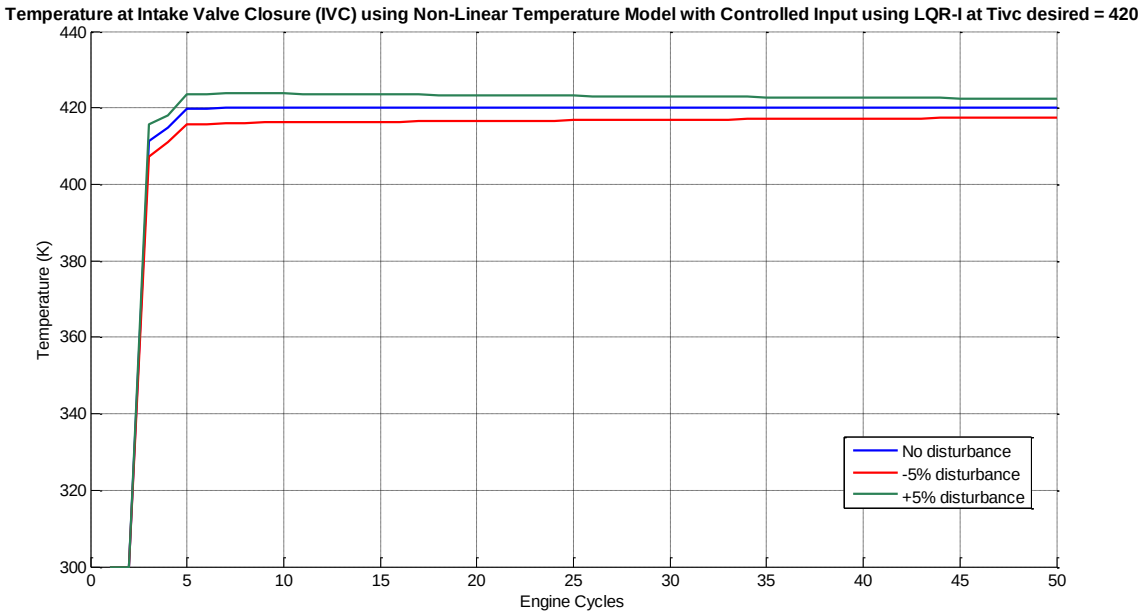

Figure 4.17 Effect of actuator disturbance on the output of the system

4.6.2 Parameter Variation

Parameter variation represents inaccuracies within certain parameters in the nonlinear model. Parameters that are subject to inaccuracies include inlet pressure, inlet temperature, and equivalence ratio. Equivalence ratio was the chosen parameter to test the effect of parameter variation on the system. The reason is that there is no control over the inlet pressure within the engine setup since no turbocharger is installed. In addition, a heater is not added at the intake duct where fresh air and fuel are mixed and therefore, there is no control over the inlet temperature. Inaccuracies in the equivalence ratio could be caused by problems with the fuel injector hence affecting the fuel flow rate.

To evaluate how well the controller can handle parameter variation, a gain of ±5% has been added to the equivalence ratio and the input and output response are plotted as shown in Figures 4.18 and 4.19, respectively. As shown in both figures, adding the disturbance caused a deviation in both input and output. Parameter variation caused a -0.36% and a 0.56% error when -5% and +5% disturbance was added, respectively. This error is quite minimal and it is also noticed that the error in the output is converging towards the desired output of 420K. Hence, this shows that the controller is rejecting the disturbance due to parameter variation as well.

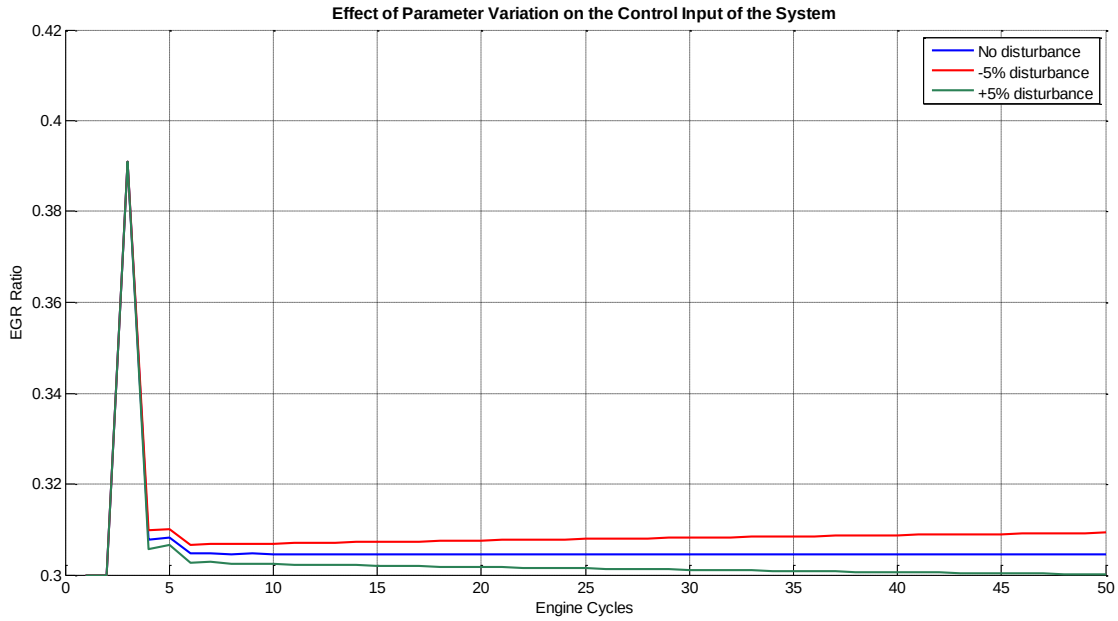

Figure 4.18 Effect of parameter variation on the control input of the system

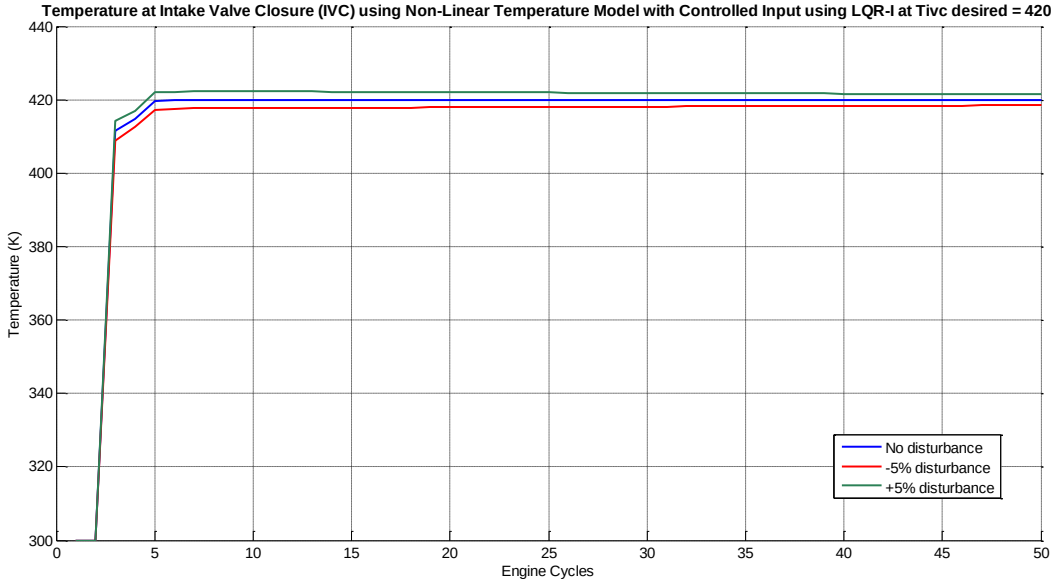

Figure 4.19 Effect of parameter variation on the output of the system

Since the start of combustion of the HCCI engine is being controlled through T_{IVC}, a temperature sensor has to be installed at the intake valve to measure the actual output. There is a possibility that the sensor output is inaccurate due to the presence of noise. Therefore, the controller is tested against the presence of white Gaussian noise with an amplitude of 5% of the measured output. Figure 4.20 shows the block diagram of the system with added noise.

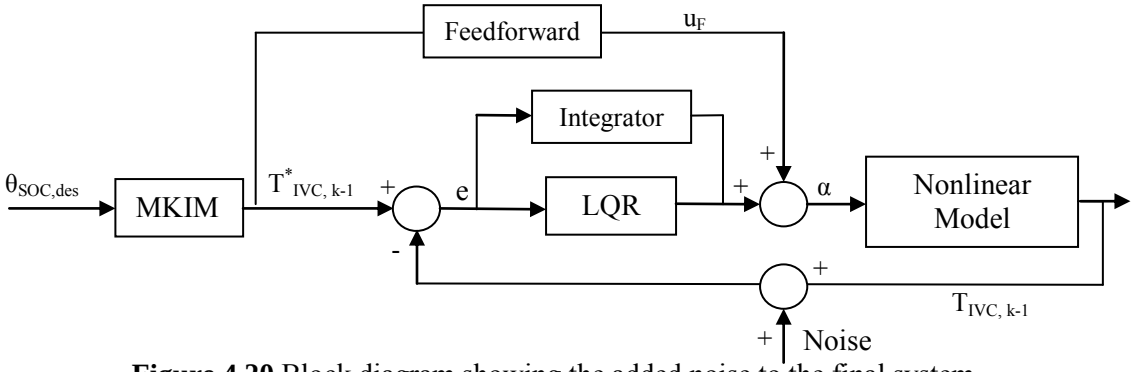

Figure 4.20 Block diagram showing the added noise to the final system

Figures 4.21 and 4.22 show the effect of adding noise to the control input and the system output, respectively. The error in the output is around 0.4%. This also shows that the controller is able to reject the noise and track the desired output with minimal error.

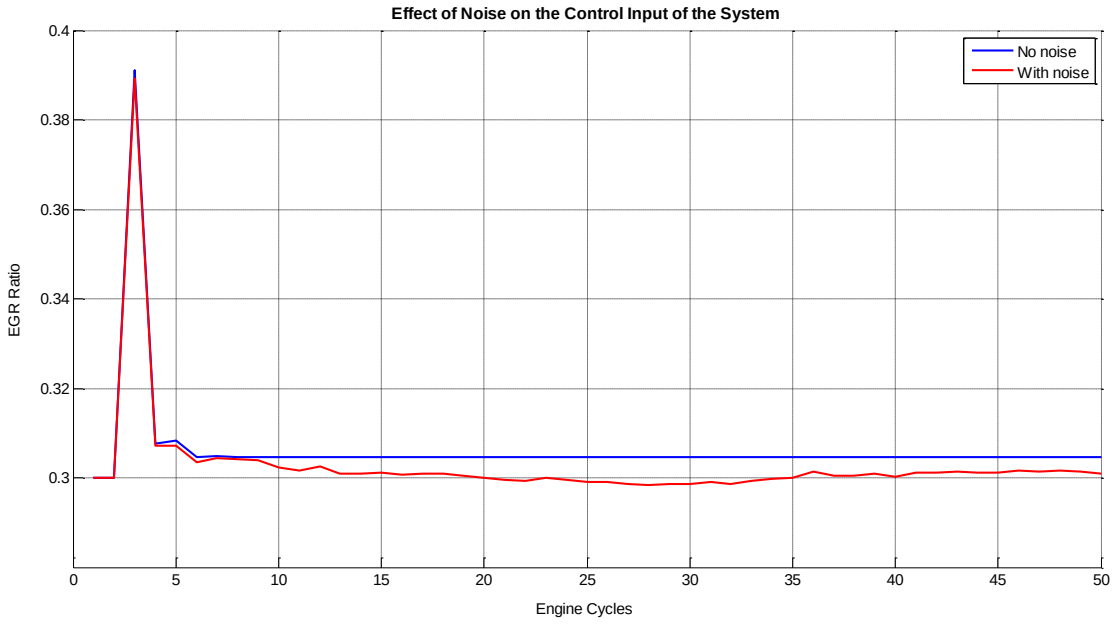

Figure 4.21 Effect of noise on the control input of the system

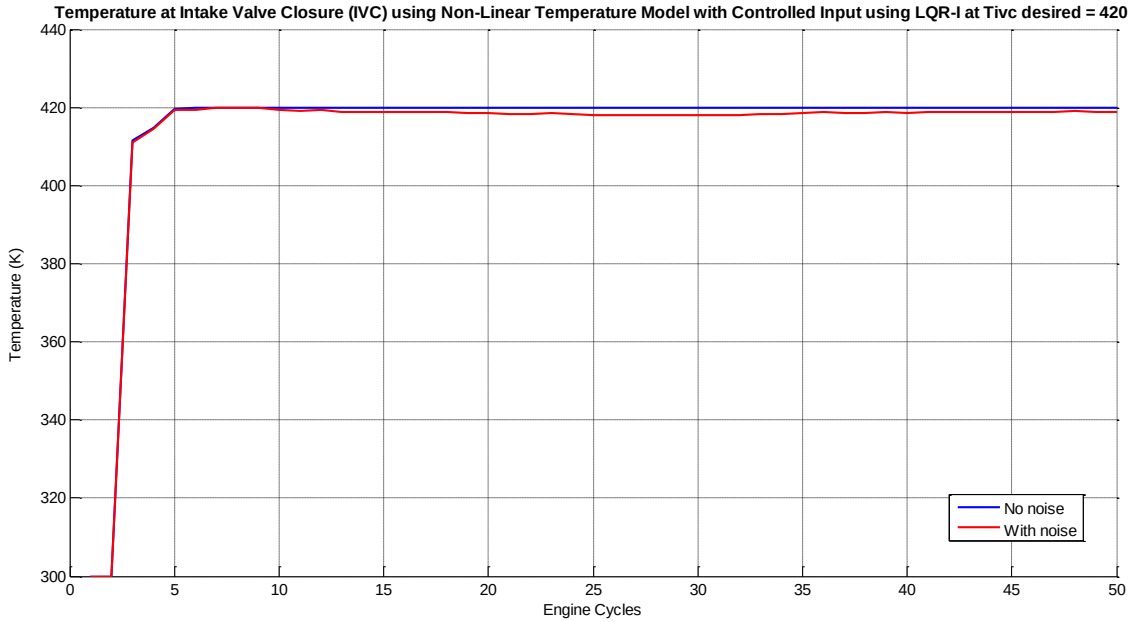

Figure 4.22 Effect of noise on the output of the system

4.7 Conclusions

LQR controllers are the most commonly used controllers that are based on optimal control approach. They are designed based on optimizing an objective function, while sustaining the stability of the closed-loop function. The gain matrix within the control law was determined to satisfy the Riccati algebraic equation.

In Section 3, it was shown that by controlling temperature at IVC through regulating the EGR valve, the combustion timing will occur at a desired timing. Therefore, the objective of the LQR controller was defined to minimize the error between the actual T_{IVC} and the desired T_{IVC} that will result in the desired θ_{SOC}. The state-space form developed in Section 3 was changed accordingly to accommodate the modified output variable. However, this modification introduced an extra term when

defining the first derivative of the state vector. This "disturbance-like" behavior was compensated through a feedforward loop added to the control law.

A MATLAB code was developed to determine the LQR gains using the system's state-space matrices and vectors. In addition, the feedforward control law was calculated through a series of assumptions. The new control law was implemented on the linear system and it succeeded in forcing the linear model to track a desired T_{IVC} value. The robustness of the LQR controller was tested by adding a disturbance to the linear system and it still managed to perform well.

After proving that the controller works well on the linear system, it was applied to the nonlinear system. The controller managed to fulfill its function by tracking the desired output with an error of 0.5%. However, it was found that this was applicable only within a certain operating range. Since linearization of the nonlinear model in Section 3 is valid only around a specific operating point, the linear model operated best around that operating point. The operating range was found to be 370K – 415k. When the control system was required to track an output outside the operating range, the error increased to more than 0.5%. Hence, an integrator was added to remove steady state error and therefore resulted in a wider operating range.

The final step was to ensure that the controller can maintain its performance in the presence of disturbance and parameter variation. An actuator disturbance was added to the EGR valve and the effect on the system output was observed. The added disturbance resulted in a deviation of less than 1% from the desired output. In addition, the error converged when simulation time increased. Additionally, a change was added

to the equivalence ratio to represent parameter variation since equivalence ratio was considered constant in engine model. A similar behavior was noticed where there was an error of less than 1% between the “disturbed” output and the desired output, and the error appeared to converge. A final disturbance was added to the temperature sensor since the controller is controlling start of combustion by measuring the temperature at IVC. This disturbance was added in the shape of white Gaussian noise. The output of the control model was also studied and it was shown that the disturbance resulted in an error of about 0.4%. Therefore, by applying such disturbances to the system, it was proved that the controller can reject them and function with minimal error.

5. CONCLUSIONS AND FUTURE WORK

This section aims to summarize and conclude the findings of this research. It also aims to discuss potential research areas for the future to further develop the scope of the project.

5.1 Summary and Conclusions

Internal combustion engines have been subjected to criticism for many years because of their contribution to global warming and human health hazards. Researchers have been trying to develop ways to improve the design of combustion engines to decrease the amount of toxic gases released into the environment. HCCI engines provided a promising solution to decrease toxic emissions while maintaining high efficiencies. However, implementation of HCCI engines is faced with a major challenge which is the control of combustion timing.

Several techniques to model and control HCCI engines have been developed. Control-oriented models have captured attention due to their short computation time and reduced complexity. In this research, the control-oriented model used for HCCI engine dynamics was modeled based on a physics-based nonlinear model in which the Modified Knock Integral Model (MKIM) correlation was used to model ignition timing. The main control technique that was used to control ignition timing is Exhaust Gas Recirculation (EGR). By circulating exhaust gases back into the engine cycle, the temperature, pressure and chemical composition of the mixture is modified hence, controlling when combustion will occur.

The engine cycle was divided into five processes and each process was represented using the first law of thermodynamics and ideal gas laws. Ignition timing was determined using the MKIM correlation and validated.

Validation was done using an engine model developed by GT-Power, a powerful simulation tool that makes extensive use of chemical kinetics and predicts combustion timing using the knock integral correlation. Ignition timing was predicted while varying intake temperature, intake pressure and EGR ratio and the model was able to reproduce similar results to GT-Power.

After validating the nonlinear model, a closed-loop control model was developed and applied. To design the control model, input, output and states of the model had to be determined. The following were the model variables:

- Input: EGR ratio, α_k
- Output: Temperature at intake valve closure, $T_{IVC,k-1}$
- States: α_{k-1} and $T_{IVC,k-1}$ (Values form the previous engine cycle of EGR ratio and temperature at intake valve closure)

After defining the model variables, an input-output relationship was developed. This relationship was based on the nonlinear thermodynamical model developed earlier. As expected, the relationship was highly nonlinear since the thermodynamical equations used were nonlinear. In order to apply a linear control model, the obtained input-output relationship was linearized. The perturbation method was used to linearize the function. This method primarily depended on substituting the model variables with their linear

expansions and then neglecting fluctuations of an order more than one due to their infinitesimal value.

A Linear Quadratic Regulator (LQR) was designed to control the temperature at IVC through regulating the EGR valve so that combustion timing occurred at a desired timing. In this regulation problem, the output was considered as the error between a desired value of T_{IVC}, $T_{IVC,des}$, and the actual value of T_{IVC}, instead of $T_{IVC,k-1}$. Hence, the aim of the controller was to minimize the tracking error. The state-space form was changed accordingly to accommodate the modified output variable. However, this modification introduced an extra term of MY^* when defining the first derivative of the state vector. This "disturbance-like" behavior was compensated through a feedforward loop added to the control law.

The final step was to determine the LQR gains of the controller. MATLAB's LQR function was used where the inputs were the system's state-space matrices and vectors. The feedforward control input was calculated by making the following assumptions:

a) The system is operating at steady-state and hence the derivatives of the states variables tend to zero.
b) The output, i.e. the error, tends to 0 since the goal of the LQR is to minimize the error.

The new control law was implemented on the linear system and it was able to accurately track the desired output. The robustness of the LQR controller was also tested against 50% disturbance added to the control input. It was shown that the output of the linear

model with and without disturbance overlapped. Hence, the controller was able perform its function well and can be implemented on the nonlinear model.

The performance of the nonlinear model was evaluated based on a 0.5% error when tracking the desired output. It was found that when varying the desired output outside the range of 370K – 400K, the error increased more than 0.5%. This was due to the fact that the linear model was linearized about operating point 4, i.e. at T_{IVC} = 390K. Hence, the linear model operated best when the desired output was around the operating point. In order to increase the operating range of the controller, an integrator was added to cancel steady-state errors. The output of the nonlinear model after adding the integrator showed that the error decreased to values less than 0.5%, therefore increasing the operating range.

It was also important to test the performance of the controller when subjected to disturbance and parameter changes. A $\pm$5% disturbance gain was added to the control input as a representation of the EGR valve not working properly. In addition, a $\pm$5% gain was added to the equivalence ratio to symbolize a variation in parameter which can be due to a problem with the fuel injector.

The addition of the disturbance to the control input resulted in a difference in the output with no disturbance and with added disturbance. The deviation in the output was within a $\pm$1% error. It was also observed that, as simulation time increased, the error converged causing the output to slowly approach the desired value. Therefore, the controller was able to slowly reject the actuator disturbance.

A similar behavior was seen when parameter variation was added to the system. The difference in the output between no disturbance and with disturbance was also within $\pm 1\%$ error and it slowly converged towards the desired output. Hence, the controller could also reject disturbances caused by parameter variation.

As a final performance test, noise was also added to the output to represent any inaccuracies caused by the in-cylinder temperature sensor. White Gaussian noise was added and the input and output of the system were studied. The addition of noise caused an error of about 0.4% and the system remained stable with no noticeable divergence from the desired output value.

In conclusion, the developed controls-oriented model, based on the MKIM correlation, was able to successfully model the combustion timing of a natural gas HCCI engine. A linear control scheme was designed to control the temperature at intake valve closure through regulation of the EGR ratio. This was proposed as an indirect method to control combustion timing. The controller was able to track a desired ignition timing with minimal error and reject any changes in the system in terms of disturbances, parameter variations, and noise.

5.2 Areas for Future Research

Although the work presented in this thesis made some steps towards controlling the ignition timing of natural gas HCCI engines, there are still some areas of improvement. The most important next step would be to apply the developed controller on an experimental setup. The controller performed well when applied to a control-oriented model. However, there are several processes that occur in a real engine that

were not taken into consideration. Therefore, it is necessary to rest the performance of the controller on a real engine.

Another area that could be further developed is the application of other control systems whether linear or nonlinear. Examples of linear control schemes that could be studied are Linear Quadratic Gaussian (LQG) controller and Linear Parameter Varying (LPV) controller. The performance of such control schemes can be compared to the developed LQR controller to evaluate which controller works best. Nonlinear control schemes could be used to maintain the nonlinearity of the developed model without resorting to linearization. It was shown in Section 4 that linearization of the nonlinear model caused limitation to the performance of the controller. Therefore, by avoiding linearzation, the performance of the designed controller can be improved. Nonlinear robust control systems such as backstepping have been used to control nonlinear systems. Therefore, it would be interesting to compare the performance of a linear and nonlinear controller when applied to the same model.

Finally, other control-oriented modeling techniques could be implemented such as system identification. Assuming that an experimental engine has been set up, experimental data could be used to identify a nonlinear or linear model to present the dynamics of the HCCI engine. The resulting model could be compared to the physics-oriented model developed in this thesis to evaluate which method was able to fully capture the dynamics of the HCCI engine.

REFERENCES

[1] Asia Development Bank, 2003, "Appendix on Adverse Health and Environmental Effects from Vehicle Emissions," Policy Guidelines for Reducing Vehicle Emissions in Asia, Manila, Philippines.

[2] EPA, U. S., 2010, "Light-Duty Vehicle and Light-Duty Truck – Tier 0, Tier 1, National Low Emission Vehicle (NLEV), and Clean Fuel Vehicle (CFV) Exhaust Emission Standards," U.S. Environmental Protection Agency, Office of Transportation and Air Quality (OTAQ), Washington, DC.

[3] EPA, U. S., 2009, "Light-Duty Vehicle, Light-Duty Truck, and Medium-Duty Passenger Vehicle – Tier 2 Exhaust Emission Standards," U.S. Environmental Protection Agency, Office of Transportation and Air Quality (OTAQ), Washington, DC.

[4] Onishi, S., Jo, S. H., Shoda, K., Jo, P. D., and Kato, S., 1979, "Active Thermo-Atmosphere Combustion (ATAC) A New Combustion Process for Internal Combustion Engines," SAE Paper No. 790501.

[5] Aceves, S. M., Flowers, D. L., Martinez-Frias, J., and Smith, R., 2001, "HCCI Combustion: Analysis and Experiments," SAE Paper No. 2001-01-2077.

[6] Stauffer, N., 2007, “MIT Researchers Work Towards Spark-Free, Fuel-Efficient Engines,” MIT Energy Initiative, MIT Laboratory of Energy and the Environment.

[7] Au, M. Y., Girard, J. W., Dibble, R., Flowers, D., Aceves, S. M., Martinez-Frias, J., Smith, R., Seibel, C., and Mass, U., 2001, "1.9-Litre Four-Cylinder HCCI Engine Operation with Exhaust Gas Recirculation," SAE Paper No. 2001-01-1894.

[8] Yao, M., Zheng, Z., and Liu, H., 2009, "Progress and recent trends in homogeneous charge compression ignition (HCCI) engines," Progress in Energy and Combustion Science, **35**, pp. 398-437.

[9] Shaver, G.M., Gerdes, J. C., Jain, P., Caton, P. A., and Edwards, C. F., 2003, "Modeling for Control of HCCI Engines," Proceedings of the American Control Conference, pp. 749-754.

[10] Fiveland, S. B., and Assanis, D. N., 2000, "A Four-Stroke Homogeneous Charge Compression Ignition Engine Simulation for Combustion and Performance Studies," SAE Paper No. 2000-01-0332.

[11] Bengtsson, J., Gafvert, M., and Strandh, P., 2004, "Modeling of HCCI Engine Combustion for Control Analysis," Proceedings of IEEE Conference on Decision and Control, pp. 1682-1687.

[12] Smith, J. R., Aceves, S. M., Westbrook, C. K., and Pitz, W. J., 1997, "Modeling of Homogeneous Charge Compression Ignition (HCCI) of Methane," Proceedings of 1997 ASME Internal Combustion Engine Fall Technical Conference, 1997-ICE-68, 29:85-90.

[13] Fiveland, S. B., and Assanis, D. N., 2001, "Development of a Two-Zone HCCI Combustion Model Accounting for Boundary Layer Effects," SAE Paper No. 2001-01-1028.

[14] Fiveland, S. B., and Assanis, D. N., 2002, "Development and Validation of a Quasi-Dimensional Model for HCCI Engine Performance and Emissions Studies under Turbocharged Conditions," SAE Paper No. 2002-01-1757.

[15] Kongsereeparp, P., Checkel, M. D., and Kashani, B., 2005, "A Stand-Alone Multi-Zone Model for Combustion in HCCI Engines," ASME International Combustion Engine Division 2005 Fall Technical Conference.

[16] Babajimopoulos, A., Assanis, D. A., and Fiveland, S. B., 2002, "Modeling the Effects of Gas Exchange Process on HCCI Combustion and an Evaluation of Potential Control through Variable Valve Actuation," SAE Paper No. 2002-01-2829.

[17] Flowers, D. L., Aceves, S. M., Martinez-Frias, J., Hessel, R., and Dibble, R., 2003, "Effect of Mixing on Hydrocarbon and Carbon Monoxide Emissions Prediction for Isooctane HCCI Engine Combustion Using A Multi-Zone Detailed Kinetics Solver, SAE Paper No. 2003-01-1821.

[18] Agarwal, A., and Assanis, D., 1998, "Multi-Dimensional Modeling of Natural Gas Ignition under Compression Ignition Conditions Using Detailed Chemistry," SAE Paper No. 980136.

[19] Agarwal, A., and Assanis, D., 2000, "Multi-Dimensional Modeling of Ignition, Combustion and Nitric Oxide Formation in Direct Injection Natural Gas Engines," SAE Paper No. 2000-01-1839.

[20] Killingsworth, N. J., Aceves, S. M., Flowers, D. L., and Krstić, M., 2006, "A Simple HCCI Engine Model for Control," IEEE International Conference on Control Applications.

[21] Rausen, D. J., Stefanopoulou, A. G., Kang, J. M., Eng, J. A., and Kuo, T. W., 2005, "A Mean-Value Model for Control of Homogeneous Charge Compression Ignition (HCCI) Engines," Journal of Dynamic Systems, Measurement, and Control, **127**, pp. 355-362.

[22] Shahbakhti, M., and Koch, C. R., 2009, "Dynamic Modeling of HCCI Combustion Timing in Transient Fueling Operation," SAE Paper No. 2009-01-1136.

[23] Shabakhti, M., and Koch, C. R., 2010, "Physics Based Control Oriented Model for HCCI Combustion Timing," Journal of Dynamic Systems, Measurement and Control, **132**, pp. 021010-1 – 021010-12.

[24] Shaver, G. M., Gerdes, J. C., Roelle, M. J., Caton, P. A., and Edwards, C. F., 2005, "Dynamic Modeling of Residual-Affected Homogeneous Charge Compression Ignition Engines with Variable Valve Actuation," ASME Journal of Dynamic Systems, Measurement, and Control, **127**, pp. 374-381.

[25] Shaver, G. M., Roelle, M. J., and Gerdes, J. C., 2006, "Modeling Cycle to Cycle Dynamics and Mode Transition in HCCI Engines with Variable Valve Actuation," IFAC Journal on Control Engineering Practice, **14**, pp. 213-222.

[26] Chiang, C. J., and Stefanopoulou, A. G., 2007, "Stability Analysis in Homogeneous Charge Compression Ignition (HCCI) Engines with High Dilution", IEEE Transactions on Control Systems Technology, **15**, pp. 209-219.

[27] Jennische, M., 2003, "Closed-Loop Control of Start of Combustion in a Homogeneous Charge Compression Ignition Engine," MS. Thesis, KTH Royal Institute of Technology, Sweden.

[28] Roy, S., Malik, O. P., and Hope, G. S., 1991, "A Least-Squares Based Model-Fitting Identification Technique for Diesel Prime-Movers with Unknown Dead-Time," IEEE Transactions on Energy Conversion, **6**, pp. 251-256.

[29] Melgaard, H., Hendricks, E., and Madsen, H., 1990, "Continuous Identification of a Four-Stroke SI Engine," Proceedings of the American Control Conference, pp. 1876-1881.

[30] Bengtsson, J., Strandh, P., Johansson, R., Tunestål, P., and Johansson, B., 2006, "Multi-Output Control of a Heavy Duty HCCI Engine using Variable Valve Actuation and Model Predictive Control," SAE Paper No. 2006-01-0873.

[31] Strandh, P., Bengtsson, J., Johansson, R., Tunestål, P., and Johansson, B., 2004, "Cycle-to-Cycle Control of a Dual-Fuel HCCI Engine," SAE Paper No. 2004-01-0941.

[32] Haraldsson, G., Tunestål, P., Johansson, B., and Hyvönen, J., 2004, "HCCI Closed-Loop Combustion Control Using Fast Thermal Management," SAE Paper No. 2004-01-0943.

[33] Killingsworth, N. J., 2007, "HCCI Engine Control and Optimization," Ph.D. Thesis, University of California, San Diego.

[34] Hyvönen, J., Haraldsson, G., and Johansson, B., 2003, "Supercharging HCCI to Extend the Operating Range in a Multi-Cylinder VCR HCCI Engine," SAE Paper No. 2003-01-3214.

[35] Haraldsson, G., Tunestål, P., Johansson, B., and Hyvönen, J., 2003, "HCCI Combustion Phasing with Closed-Loop Combustion Control Using Variable Compression Ratio in a Multi-Cylinder Engine," SAE Paper No. 2003-01-1830.

[36] Law, D., Kemp, D., Allen, J., Kirkpatrick, G., and Copland, T., 2000, "Controlled Combustion in an IC-Engine with a Fully Variable Valve Train," SAE Paper No. 2000-01-0251.

[37] Caton, P., Simon, A., Gerdes, J. C., and Edwards, C., 2003, "Residual-effected Homogeneous Charge Compression Ignition at Low Compression Ratio Using Exhaust Reinduction," International Journal of Engine Research, **4**, pp. 163-177.

[38] Agrell, F., Ångström, H. E., Eriksson, B., Wikander, J., and Linderyd, J., 2003, "Integrated Simulation and Engine Test of Closed-Loop HCCI Control by Aid of Variable Valve Timings," SAE Paper No. 2003-01-0748.

[39] Johansson, T., Johansson, B., Tunestål, P., and Aulin, H., 2009, "HCCI Operating Range in a Turbo-Charged Multi Cylinder Engine with VVT and Spray-Guided DI," SAE Paper No. 2009-01-0494.

[40] Christensen, M., Johansson, B., Amnéus, P., and Mauss, F., 1998, "Supercharged Homogeneous Charge Compression Ignition," SAE Paper No. 980787.

[41] Martinez-Frias, J., Aceves, S. M., Flowers, D., Smith, J. R., and Dibble, R., 2001, "Equivalence Ratio-EGR Control of HCCI Engine Operation and the Potential for Transition to Spark-ignited Operation," SAE Paper No. 2001-01-3613.

[42] Chen, R., and Milovanovic, N., 2002, "A Computational Study into the Effect of Exhaust Gas Recycling on Homogeneous Charge Compression Ignition Combustion in Internal Combustion Engines Fuelled with Methane," International Journal of Thermal Sciences, **41**, pp. 805-813.

[43] Hillion, M., Chauvin, J., Grondin, O., and Petit, N., 2008, "Active Combustion Control of Diesel HCCI Engine: Combustion Timing," SAE Paper No. 2008-01-0984.

[44] Morsy, M. H., and Chung, S. H., 2007, "Effect of Additives on Ignition of Methane at Homogeneous Charge Compression Ignition Engine-like Conditions," Journal of Automobile Engineering, **221**, pp. 605-619.

[45] Hu, H., Wilson, T., Richardson, S., Wyszynski, M. L., Megaritis, T., Yap, D., Golunski, S., and James, D., 2004, "Extension of the Boundary of HCCI Combustion Using Fuel Reforming Technology," SAE Paper No. 2004-08-0286.

[46] Olsson, J., Tunestål, P., and Johansson, B., 2001, "Closed-loop Control of an HCCI Engine," SAE Paper No. 2001-01-1031.

[47] Agrell, F., Ångström, H. E., Eriksson, B., Wikander, J., and Linderyd, J., 2005, "Control of HCCI during Transients by Aid of Variable Valve Timings Through the Use of Model Based Non-Linear Compensation," SAE Paper No, 2005-01-0131.

[48] Shaver, G. M., and Gerdes, J. C., 2003, "Cycle-to-cycle Control of HCCI Engines," Proceedings of the 2003 ASME International Mechanical Engineering Congress and Exposition, IMECE2003-41966.

[49] Shaver, G. M., Roelle, M., and Gerdes, J. C., 2005, "Decoupled Control of Combustion Timing and Work Output in Residual-affected HCCI Engines," Proceedings of American Control Conference, pp. 3871-3876.

[50] Shaver, G. M., Gerdes, J. C. and Roelle, M., 2004, "Physics-based Closed-loop Control of Phasing, Peak Pressure, and Work Output in HCCI Engines Utilizing Variable Valve Actuation," Proceedings of American Control Conference, pp. 150-155.

[51] Ravi, N., Roelle, M. J., Jungkunz, A. F., and Gerdes, J. C., 2006, "A Physically Based Two-state Model for Controlling Exhaust Recompression HCCI in Gasoline Engines," Proceedings of the 2006 ASME International Mechanical Engineering Congress and Exposition, IMECE2006-15331.

[52] U.S. Energy Information Administration, 2011, "Qatar Energy Data, Statistics and Analysis – Oil, Gas, Electricity, Coal,", http://www.eia.gov/countries/cab.cfm?fips=QA

[53] Heywood, J. B., 1988, *Internal Combustion Engine Fundamentals*, McGraw-Hill, New York.

[54] Swan, K., Shahbakhti, M., and Koch, C. R., 2006, "Predicting Start of Combustion Using a Modified Knock Integral Method for an HCCI Engine," SAE Paper No. 2006-01-1086.

[55] Mortimer, M., and Taylor, P., 2002, *Chemical Kinetics and Mechanism, Volume 1*, Royal Society of Chemistry, Great Britain.

[56] Assanis, D. N., Filipi, Z. S., Fiveland, S. B., and Syrimis, M., 2003, "A Predictive Ignition Delay Correlation Under Steady-State and Transient Operation of a Direct Injection Diesel Engine," Journal of Engineering for Gas Turbines and Power, **125**, pp. 450-457.

[57] Ogink, R., 2005, "Approximation of Detailed-Chemistry Modeling by a Simplified HCCI Combustion Model," SAE Paper No. 2005-24-037.

[58] He, X., Donovan, M., Zigler, B., Palmer, T., Walton, S., Wooldridge, M., and Atreya, A., 2005, "An Experimental and Modeling Study of Iso-Octane Ignition Delay Times under Homogeneous Charge Compression Ignition Conditions," Combustion and Flame, **142**, pp. 266-275.

[59] Babajimopoulos, A., Lavoie, G., and Assanis, D., 2007, "On the Role of Top Dead Center Conditions in the Combustion Phasing of Homogeneous Charge Compression Ignition Engines," Combustion Science and Technology, **179**, pp. 2039-2063.

[60] Livengood, C. J., and Wu, C. P., 1955, "Correlation of Autoignition Phenomena in Internal Combustion Engines and Rapid Compression Machines," Proceedings of Fifth International Symposium on Combustion, The Combustion Institute, Pittsburgh, PA, pp. 347-356.

[61] Personal communication, Dr. Jerald Caton and Junnian (Daniel) Zheng, Mechanical Engineering Department, Texas A&M University, College Station, TX.

[62] Nelder, J.A., and Mead, R., 1965, "A Simplex Method for Function Minimization," Computer Journal, **7**(4), pp. 308-313.

[63] Friedland, B., 2005, *Control System Design: An Introduction to State-Space Methods*, Dover Publications Inc., Mineola, New York.

[64] Zhou, K., Doyle, J. C., and Glover, K., 1996, *Robust and Optimal Control*, Prentice Hall, New Jersey.

VITA

Name: Marwa Walid Fathy AbdelGawad

Address: c/o Ahmad Ahmed
182-21 150th Avenue
DOH 2058
Springfield Gardens, NY 11413

Email Address: mwalid@aucegypt.edu

Education: B.Sc., Mechanical Engineering, The American University in Cairo, 2007